Tritium β-decay in pionless effective field theory

Hilla De-Leon,[1,*] Lucas Platter,[2,3,†] and Doron Gazit[1,‡]

[1] *Racah Institute of Physics, The Hebrew University, 9190401 Jerusalem, Israel*
[2] *Department of Physics and Astronomy, University of Tennessee Knoxville Knoxville, TN 37996, USA*
[3] *Physics Division, Oak Ridge National Laboratory, Oak Ridge, TN 37831, USA*

(Dated: December 1, 2016)

We calculate the β-decay of tritium, *i.e.*, of its ^{3}H nucleus (triton), at next-to-leading order in pionless effective field theory. At this order a low-energy parameter L_{1A} enters the calculation that is also relevant for a high-accuracy prediction of the solar proton-proton fusion rate. We show proper renormalization of our perturbative calculation by an analysis of the residual cutoff dependence in observables. We find that next-to-leading order corrections contribute about 1% to the triton decay Gamow-Teller strength. We show that these conclusions are insensitive to different arrangements of the effective range expansion. We use these to fix L_{1A} to high accuracy, and provide reliable theoretical and experimental uncertainty estimates.

arXiv:1611.10004v1 [nucl-th] 30 Nov 2016

I. INTRODUCTION

Electroweak observables of nuclei, such as transitions, magnetic moments and β-decay rates are used to probe unique properties of the nuclear force. In recent years, an effort has begun to calculate such observables using effective field theory (EFT) approaches. In EFT, the ratio of two separated scales is used as an expansion parameter in a systematic low-energy expansion in the calculation of observables. The low-energy scale is usually a small momentum scale Q while the second scale $\Lambda_{\rm cut}$ is frequently related to the lightest exchange particle or lowest lying excitation not included in the theory. The EFT then has to preserve all symmetries of the fundamental theory and the resulting Lagrangian includes only the relevant degrees of freedom while heavier excitations are integrated out of the theory. Thus, one can obtain an expression of non-renormalizable interactions which can be organized as a power series in $Q/\Lambda_{\rm cut}$ [1–5].

Chiral effective field theory identifies the pion as a Goldstone boson of spontaneously broken chiral symmetry of QCD, stemming from the small masses of the up and down quarks. The finite mass of the pion originates from the explicit chiral symmetry breaking, *i.e.* the nonzero up and down quark masses. This framework has been used to construct a nuclear interaction that describes nuclear spectra and scattering observables to very high accuracy [6]. It has also been used to construct the nuclear electroweak current operator and for subsequent calculations [7, 8]. These calculations have highlighted the benefit of an approach in which current operators and the interaction between nucleons are treated consistently. The electroweak properties of the three-nucleon system are particularly important since these observables can be used to constrain parameters in the three-nucleon force of chiral effective theory.

The so-called pionless EFT ($\not\pi$EFT) is an alternative EFT approach to light nuclei that is particularly useful at the low energies that are of interest for astrophysical processes, *i.e.* $Q \sim 10$ MeV $\ll m_\pi = 140$ MeV. The interactions in $\not\pi$EFT are constructed using only contact interactions, and the pion mass sets therefore the breakdown scale of this approach [9, 10]. Using this theory all particles but nucleons are "integrated out". In addition, the strong interaction characterizing QCD at low energies, leads to a scale separation between the scattering length a and the range of the interaction R. $\not\pi$EFT exploits this ratio as an expansion parameter. Thus, $\not\pi$EFT at leading order is a quantum field theoretical formulation of the zero-range limit, in which the range of an interaction is taken to zero. As a consequence, a three-body force is needed at leading order for the description of three-nucleon systems within this framework, that is directly related to the well-known Efimov effect [11, 12]. Since the binding energies of nuclei with $A \leq 3$ are small (*i.e.* $E_B < 10$ MeV), those nuclei can indeed be described using $\not\pi$EFT [12].

The Coulomb interaction in light nuclei is an additional complication. The Coulomb interaction is nonperturbative at low momenta $\lesssim 10\,\frac{\rm MeV}{\rm c}$, as can be seen in the strong renormalization of the proton-proton scattering length, but should be perturbative in nuclei where the typical momenta are much higher. ^{3}He is the lightest, and therefore simplest, nucleus to test the combination of $\not\pi$EFT and Coulomb interaction [13–15] and many recent works have discussed this problem. In particular, it was shown that while at leading order (LO) ^{3}He is described correctly within $\not\pi$EFT, at next-to-leading order (NLO) the results are not so clear, and some approaches have shows the need for additional, isospin dependent, three-body forces. Then additional three-nucleon observables are needed to obtain predictive power within $\not\pi$EFT at NLO [16–18].

One of the ways to additionally test the predictions of $\not\pi$EFT for the structure of the three-nucleon system at NLO is through the aforementioned electroweak properties of light nuclear systems. This is the goal of this paper in which we aim at describing tritium β-decay. This ob-

* E-mail: hilla.deleon@mail.huji.ac.il
† E-mail: lplatter@utk.edu
‡ E-mail: doron.gazit@mail.huji.ac.il

servable is particularly interesting since it is well-known experimentally, and can be used to determine the short-range strength of the axial coupling to nuclei, required for a high-accuracy description of the astrophysically relevant proton-proton fusion rate [19–22]. In the context of ∉EFT , this coupling at NLO is represented by a low-energy constant L_{1A}, whose exact value is a matter of discussion in the literature [23–28]. The large uncertainty in the current determination of L_{1A} is the source of this discussion. It is thus called for to check the triton decay within ∉EFT , as a method to fix this parameter [29]. Moreover, this provides additional EFT checks, which were not considered in the context of triton decay to date, such renormalization group invariance, convergence pattern of the EFT, and existence of terms with large fluctuations within the NLO contribution.

The paper is organized as follows. The general formalism of ∉EFT is presented in Section 2. The equations giving the three-nucleon wave functions for (^{3}H and ^{3}He) and a diagrammatic representation of the three-nucleon wave function normalization coefficients are given in Section 3. The general form of a calculation of a matrix element between two $A = 3$ bound state amplitudes is shown in Section 4. The NLO corrections to the Faddeev equation are discussed in Section 5. These NLO solutions are used as platform to the calculation of weak matrix elements, as presented in Section 6. In Section 7, we use the experimental value of the triton β decay rate to fix L_{1A} at NLO. In Section 8, we discuss this approach of matching this counterterm in comparison to previous studies. We then summarize and provide an outlook in Section 9.

II. THE TWO-NUCLEON SYSTEM UP TO NEXT-TO-LEADING ORDER

In this section, we briefly summarize the theoretical formalism employed here to calculate the properties of the two-nucleon system in the spin-singlet and triplet channels. We use a formulation of ∉EFT with dynamical dimer fields t and s. The fields t and s have the quantum numbers of two coupled nucleons in an S-wave spin triplet and singlet state, respectively. This formulation is just a Hubbard-Stratonovich transformation of the usual single nucleon theory but simplifies the calculation of three-body amplitudes. The Lagrangian that we use has the form [30]:

$$\begin{aligned}\mathcal{L} =& N^\dagger\left(iD_0+\frac{\mathbf{D}^2}{2M}\right)N - t^{i\dagger}\left[\sigma_t+\left(iD_0+\frac{\mathbf{D}^2}{4M}\right)\right]t^i \\ & - s^{A\dagger}\left[\sigma_s+\left(iD_0+\frac{\mathbf{D}^2}{4M}\right)\right]s^A \\ & + y_t\left[t^{i\dagger}\left(N^T P_t^i N\right)+h.c\right] \\ & + y_s\left[s^{A\dagger}\left(N^T P_s^A N\right)+h.c\right]+\ldots,\end{aligned} \tag{1}$$

where A denotes the isospin triplet index, i the spin triplet index and N is the *single* nucleon field. The nucleon mass is denoted by M and the projection operators

$$P_t^i=\frac{1}{\sqrt{8}}\sigma^2\sigma^i\tau^2,\quad P_s^A=\frac{1}{\sqrt{8}}\sigma^2\tau^2\tau^A\ , \tag{2}$$

project on the spin-triplet and spin-triplet channel, respectively.

We use a powercounting that is appropriate for systems with a scattering length a that is large compared to the range of the interaction R [31]. Thus, the fully dressed dimer propagator is a result of summing over all nucleon-nucleon loops to all orders (Fig. 1) and is given by

$$\begin{aligned}\mathcal{D}_{t,s}^{full}(q_0,\mathbf{q}) =& \frac{4\pi}{My_{t,d}^2}\left[\frac{1}{a_{t,s}}-\sqrt{-Mq_0+\frac{\mathbf{q}^2}{4}}\right. \\ & \left.+\frac{\rho_{t,s}}{2}\left(\mathbf{q}^2/4-Mq_0\right)\right]^{-1},\end{aligned} \tag{3}$$

where $a_{t,s}$ denotes the spin triplet and singlet scattering length and $\rho_{t,s}$ is the effective range.

Matching the propagator above to the two-nucleon scattering amplitude gives renormalization conditions for the LECs in Eq. (1):

$$y^i=\frac{\sqrt{8\pi}}{M\sqrt{r_0^i}}\ , \tag{4}$$

$$\sigma^i=\frac{2}{Mr^i}\left(\frac{1}{a^i}-\mu\right)\ , \tag{5}$$

where μ is a renormalization scale entering through the power divergence subtraction (PDS) scheme employed here in the two-body sector [3, 31].

The dimer propagator shown above has two poles. One corresponds to the *physical* bound state (virtual) pole that results from the large scattering length in the triplet (singlet) channel. The other pole is a spurious pole whose energy scale lies beyond the breakdown scale of the EFT. We expand the propagator in Eq. (1) in powers of the effective range since the spurious pole causes problems in calculations for few-body systems. Through this expansion we can also isolate the piece that is exactly linear in the effective range, and treat it as NLO. We obtain at first order in this expansion

$$\begin{aligned}\mathcal{D}_{t,s}^{NLO}(q_0,\mathbf{q}) =& \frac{4\pi}{My_t^2}\left(\frac{1}{a_{t,s}}-\sqrt{-Mq_0+\frac{\mathbf{q}^2}{4}}\right)^{-1} \\ & \times\left[1-\frac{\rho_{t,s}}{2}\left(\sqrt{\mathbf{q}^2/4-Mq_0}+\frac{1}{a_{t,s}}\right)\right].\end{aligned} \tag{6}$$

The deuteron normalization is given by [30]:

$$Z_d^{-1}=i\frac{\partial}{\partial_{p_0}}\frac{1}{i\mathcal{D}_t(p_0,p)}\Big|_{p_0=-\frac{\gamma_t^2}{M},p=0}. \tag{7}$$

We obtain for the fully dressed dimer propagator

$$Z_d = \frac{1}{1-\gamma_t\rho_t} = \underbrace{1}_{\rm LO} + \underbrace{\gamma_t\rho_t}_{NLO} + \underbrace{(\gamma_t\rho_t)^2}_{N^2LO} + \underbrace{(\gamma_t\rho_t)^3}_{N^3LO} + ... \\ = 1.69 \tag{8}$$

This result for the perturbative expansion of the Z-factor is based on a matching of the parameters in the EFT to the effective range expansion (ERE). At NLO the parameters can also be chosen to fix the pole position and residue of the triplet two-body propagator to the deuteron values. This parameterization is known as the Z-parameterization and is advantageous because it reproduces the correct residue about the deuteron pole at NLO, instead of being approached perturbatively order by-order as in ERE parameterization [24, 32–35].

Using the Z-parameterization, instead of the convergence displayed in Eq. (8), leads to: [24, 32–35]:

$$Z_d = \underbrace{1}_{\rm LO} + \underbrace{Z_d - 1}_{NLO} + \underbrace{0}_{N^2LO} + \underbrace{0}_{N^3LO} + ... = 1.69. \tag{9}$$

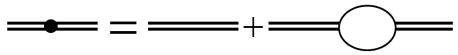

FIG. 1. The dressed dibaryon propagator. The bare dibaryon propagator is dressed by nucleon bubbles to all orders.

A. Proton-proton dibaryon and renormalization of the Coulomb effects

The derivation of the proton-proton (pp) dibaryon up to NLO is based on [24, 36, 37].

At LO, the pp self-energy contains an infinite series of ladder diagrams of Coulomb photon exchanges. Due to the non-perturbative nature of the Coulomb interaction at low energies, those diagrams have to be resummed up to infinity.

The LO Coulomb propagator is given by:

$$i\mathcal{D}_{pp}(p) = \frac{i4\pi}{My_s^2}\frac{1}{\frac{1}{a_p} + H(\eta)}\ , \tag{10}$$

where a_p denotes the proton-proton scattering length in the modified effective range expansion (recall that S-wave proton-proton scattering can only occur in the spin-singlet channel) and the function H is

$$H(\eta) = \psi(i\eta) + \frac{1}{2i\eta} - \ln(i\eta). \tag{11}$$

The function ψ is the logarithmic derivative of the Γ-function.

The NLO correction to the Coulomb propagator is given by the diagrams shown in Fig. 2. By summing

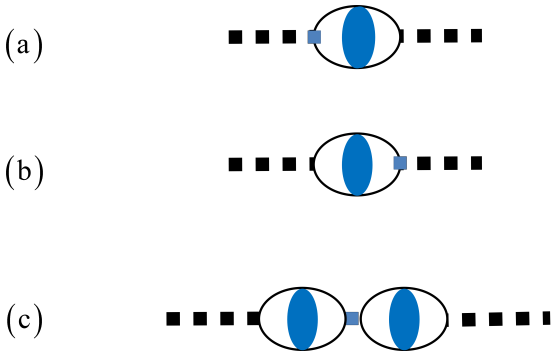

FIG. 2. The pp dibaryon propagator up to next-to-leading order. The blue square denotes the NLO insertion of the effective range.

over all contributions, the NLO Coulomb propagator is given by

$$\mathcal{D}_{pp}^{NLO}(p) = -\frac{2\pi\rho_C}{My_s^2}\frac{p^2-\alpha\mu M}{\left[\frac{1}{a_p}+H(\eta)\right]^2} = \\ -\frac{4\pi}{My_s^2}\frac{1}{\frac{1}{a_p}+H(\eta)}\left[\frac{\rho_C}{2}\left(\frac{p^2-\alpha\mu M}{\frac{1}{a_p}+H(\eta)}\right)\right] = \\ -D_{pp}^{LO}(p)\frac{\rho_C}{2}\left(\frac{p^2-\alpha\mu M}{\frac{1}{a_p}+H(\eta)}\right) \tag{12}$$

III. THE THREE-NUCLEON SYSTEM

In this section we describe the calculation of the bound state amplitudes that are required for the calculation of the weak matrix elements considered in this work.

A. The three-nucleon system at leading order

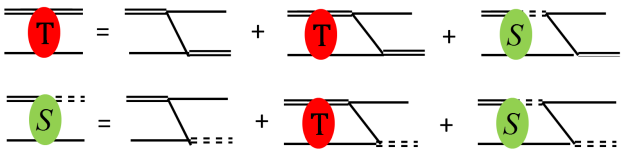

FIG. 3. (Color online) n-d scattering with a 3-body force. The double line is a propagator of the two intermediate auxiliary fields D_t (solid) and D_s (dashed). The red bubble (T) represents the triplet channel T=0, S=1, while the green bubble (S) represents the singlet channel T=1, S=0.

Neutron-deuteron S-wave scattering can occur in two channels. Either the quartet channel, in which the spin of neutron and deuteron are coupled to $S = 3/2$, or the doublet channel, with total spin $S = 1/2$. AT LO

The three-nucleon can be coupled only to the doublet channel, which includes two dimer channels: T - the spin triplet (deuteron) and S the spin singlet (np,nn,pp). Figure 3 shows a diagrammatic representation of the coupled-channel integral equation for the two scattering amplitudes T and S in the doublet channel. The Faddeev equation for ^{3}H can be written as [12, 16]:

$$\begin{aligned} T(k,p,E) &= y_t^2\left[K_1(k,p)\right] \\ &\int \delta_t(q,E)T(k,q,E)K_1(q,p,E)\frac{q^2}{\pi}dq - \\ &3\frac{y_t}{y_s}\int \delta_s(E,q)S(k,q)K_1(q,p,E)\frac{q^2}{\pi}dq\ , \end{aligned} \tag{13}$$

$$\begin{aligned} S(k,p,E) &= -3y_t y_s\left[K_1(k,p)\right] \\ &+ \int \delta_s(E,q)S(k,q)K_1(q,p,E)\frac{q^2}{\pi}dq \\ &- 3\frac{y_s}{y_t}\int \delta_t(q,E)T(k,q,E)K_1(q,p,E)\frac{q^2}{\pi}dq. \end{aligned} \tag{14}$$

Eqs. (13) and (14) can be written in matrix form:

$$t^{LO}(k,p,E) = B_0 + K_0^{(S)}(q,p,E)\otimes t^{LO}(k,p,E)\ , \tag{15}$$

where we combined the two channels into one column vector:

$$t^{LO}(k,q,E) = \begin{pmatrix} T(k,q,E) \\ S(k,q,E)\end{pmatrix}, \tag{16}$$

and have defined the operation:

$$A(...,q)\otimes B(q,...) = \int A(..,q)B(q,...)\frac{q^2}{2\pi^2}dq. \tag{17}$$

The inhomogeneous part of the integral equation is given by:

$$B_0 = Q_0\left(\frac{k^2+p^2-ME}{kp}\right)\times\begin{pmatrix} \frac{y_t^2}{2kp} \\ \frac{-3y_t y_s}{2kp}\end{pmatrix}. \tag{18}$$

The kernel is,

$$\begin{aligned} K_0^S(q,k,E) &= K_1(q,k,E) \\ &\times\begin{pmatrix} My_t^2D_t(E,q) & -3My_ty_sD_s(E,q) \\ -3My_ty_sD_t(E,q) & My_s^2D_s(E,q)\end{pmatrix} \\ &+\frac{H(\Lambda)M}{\Lambda^2}\begin{pmatrix} y_t^2D_t(E,q) & -y_ty_sD_s(E,q) \\ -y_ty_sD_t(E,q) & y_s^2D_s(E,q)\end{pmatrix}\ , \end{aligned} \tag{19}$$

where

$$K_1(k,q,E) = \frac{1}{2pk}Q_0\left(\frac{p^2+k^2-ME}{pk}\right)\ , \tag{20}$$

$$\tag{21}$$

with

$$Q(\mathrm{a}) = \frac{1}{2}\int_{-1}^{1}\frac{1}{x+a}dx\ , \tag{22}$$

$$D(E,q) = \mathcal{D}\left(E-\frac{q^2}{2M},\mathbf{q}\right)\ , \tag{23}$$

and

$$\delta_{t,s}(E,q) = \frac{My_{t,s}^2}{4\pi}D_{t,s}\left(E,q\right). \tag{24}$$

Here, E denotes the total energy of the three-body system. The term $H(\Lambda)/\Lambda^2$ denotes a three-body force that renders the three-body system cutoff independent and thereby renormalizable [11].

B. Normalization of the three-nucleon amplitude

In this section, we discuss the calculation of the three-nucleon bound state amplitude and that of its normalization. The calculation of the bound state normalization has a diagrammatic representation which is equivalent to the matrix element of the identity operator, *i.e.* summing over all the possible diagrams between two identical nuclear amplitudes. Such a diagrammatic representation will be used later in the calculation of the β-decay three-nucleon matrix element.

1. The Faddeev equation for the bound state

The above sections describe the Faddeev equation for the three-nucleon system at arbitrary energy. For negative energies, *i.e* when $E<0$ the scattering amplitude has the form

$$t(k,q,E) = \frac{\mathcal{B}(q,E)\mathcal{B}(k,E)}{E-E_B}\ , \tag{25}$$

when the energy is close to the energy of a bound state - E_B. The amplitude $t(k,q,E)$ has a residual which is regular close to the pole position and thus can be neglected for $E\to E_B$. By substituting Eq. (25) into (15), Eq. (15) becomes

$$\mathcal{B}(p,E) = K_0^{(S)}(q,p,E)\otimes\mathcal{B}(q,E)\ , \tag{26}$$

i.e. the homogeneous integral equation that has the form of the non-relativistic Bethe-Salpeter equation.

2. The non-relativistic Bethe-Salpeter wave function in a diagrammatic form

The normalization condition is given by Eq. (A-131) in Appendix A (see also Ref. [38]).

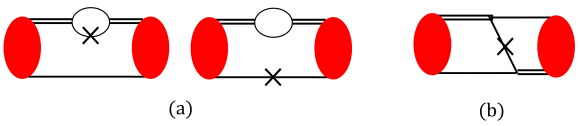

FIG. 4. (Color online) The diagrammatic representation of normalization of the homogeneous three-body Bethe-Salpeter wave functions. The double line denotes a dibaryon propagator. The cross denotes the insertion of the unity operator.

In our notation, Eq. (A-131) takes the form:

$$1 = (\mathcal{B}(q))^T \otimes \left\{ \mathcal{D}(q) \left[\frac{d}{dE} \left(\hat{I} - \mathcal{K} \right)_{E=E_B} \right] D(q') \right\} \otimes \mathcal{B}(q'). \tag{27}$$

Where:

$$\hat{I} = \frac{2\pi^2}{q^2} \delta(q - q') \mathcal{D}(q, E)^{-1}. \tag{28}$$

We note that

$$\frac{\partial}{\partial E} \left(\frac{1}{D_{t,s}(E,q)} \right) = \frac{M y_{t,s}^2}{4\pi \sqrt{3q^2/4 - 4ME}} , \tag{29}$$

and

$$\frac{\partial Q_0(q,q',E)}{\partial E} = \frac{Mq'q}{q^2 \left(q'^2 - 2ME \right) + \left(q'^2 - ME \right)^2 + q^4}. \tag{30}$$

This leads to the result that for both Eqs. (29) and (30) the energy derivative of both $\hat{I}$ and $\mathcal{K}$ is equivalent to an insertion of an additional single nucleon propagator as shown in Fig. 4 (the closed form of the two bubbles represents the integral over q and q').

Fig. 4 is the diagrammatic representation of all the possible connections between two identical bound state amplitudes $\mathcal{B}$, and therefore it is the diagrammatic form of the matrix element of the identity operator, which is just the normalization of bound state nuclear amplitude.

C. The ^{3}H bound state amplitude at LO

The three-body bound state amplitude is the solution of the homogeneous parts of Faddeev equation [39, 40]. Our calculations are carried out with the experimental data shown in Tab. I. In particular, we will be setting $a_{nn} = a_{np} = a_s$ and $S_{np} = S_{nn} = S$ (where S is the singlet channel of the scattering amplitude).

For the case of ^{3}H bound state, we express the amplitude as

$$\mathcal{B}(p,E) = \begin{pmatrix} \Gamma_T(p,E) \\ \Gamma_S(p,E) \end{pmatrix} , \tag{31}$$

where Γ_T, Γ_S denote the two bound state amplitudes that either have an outgoing/incoming spin-triplet or spin-singlet dimer, respectively.

For the triton, one needs to solve the integral equation:

$$\begin{pmatrix} \Gamma_T \\ \Gamma_S \end{pmatrix} = K_1(k,q,E) \times \begin{pmatrix} y_t^2 D_t(E,q) & -3 y_t y_s D_s(E,q) \\ -3 y_t y_s D_t(E,q) & y_s^2 D_s(E,q) \end{pmatrix} \otimes \begin{pmatrix} \Gamma_T \\ \Gamma_S \end{pmatrix}. \tag{32}$$

In order to find the value of the three-body force counterterm $H(\Lambda)$, we solve the homogeneous integral equation (*i.e.* Eq. (32)) numerically and use the known binding energy of the triton $-E_{^3\mathrm{H}} = -8.48$ MeV to remove the Λ dependence of $-E_{^3\mathrm{H}}$.

D. Helium-3 bound state amplitude at LO

1. *Adding a Coulomb interaction*

Helium-3 is the isospin partner of tritium, containing one neutron and two protons.

The photon Lagrangian is given by [16]:

$$\mathcal{L}_{photon} = -\frac{1}{4} F^{\mu\nu} F_{\mu\nu} - \frac{1}{\xi} \left(\partial_\mu A^\mu - \eta_\mu \eta_\nu \partial^\nu A^\mu \right)^2 , \tag{33}$$

which only keeps contributions from Coulomb photons. These correspond to a static Coulomb potential between two charged particles. For convenience we introduce Feynman rules for a Coulomb photon propagator:

$$i\mathcal{D}_{photon}(\mathbf{k}) = \frac{i}{\mathbf{k}^2 + \lambda}, \tag{34}$$

which we draw as a wavy line. λ is a small photon mass in order to regulate the singularity of the propagator at zero momentum transfer [16].

2. *Coulomb diagrams power counting*

The Coulomb diagrams which contribute to $p-d$ scattering are shown in Fig. 5. Naïvely all the diagrams should contain an infinite sum of photons exchange. However, we identify the binding momentum Q as the typical momentum scale for ^{3}He

$$Q \geq \sqrt{M E^B_{^3\mathrm{He}}} \simeq 85\mathrm{MeV}. \tag{35}$$

The Coulomb parameter η [36]:

$$\eta(Q) = \frac{\alpha M}{2Q} \ll 1. \tag{36}$$

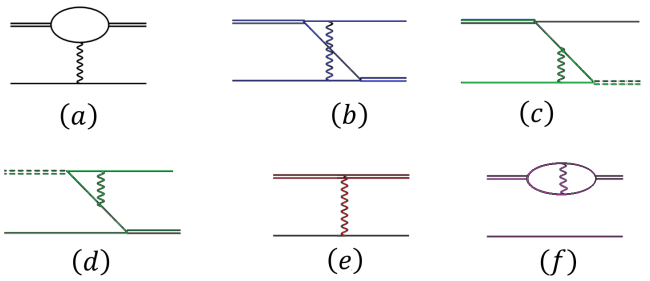

FIG. 5. The possible one-photon exchange diagrams

In the case that $\eta(Q) \ll 1$ we can treat the Coulomb interaction as a perturbation and take into account only one photon exchange diagrams.

Specifically, the fine-structure constant $\alpha \sim 1/137$, will be used as an additional expansion parameter.

The power counting for the diagrams shown in Fig. 5 are [13, 41]:

- For diagram a: $\left(\frac{\Lambda}{M^2}\right) \times \left(\frac{M}{Q^2}\right)^3 \times Q^3 \times \frac{Q^2}{M} \times \frac{\alpha}{p^2} = \frac{\Lambda}{Q}\frac{\alpha}{p^2} = \mathcal{O}((\mathcal{K})) \times \frac{\alpha M}{p}\frac{Q}{p}$
- For diagram b: $\left(\frac{\Lambda}{M^2}\right) \times \left(\frac{M}{Q^2}\right)^3 \times Q^3 \times \frac{Q^2}{M} \times \frac{\alpha}{Q^2} = \frac{\Lambda}{Q}\frac{\alpha}{Q^2} = \mathcal{O}((\mathcal{K})) \times \frac{\alpha M}{Q}$
- For diagram c: $\left(\frac{\Lambda}{M^2}\right) \times \left(\frac{M}{Q^2}\right)^3 \times Q^3 \times \frac{Q^2}{M} \times \frac{\alpha}{Q^2} = \frac{\Lambda}{Q}\frac{\alpha}{Q^2} = \mathcal{O}((\mathcal{K})) \times \frac{\alpha M}{Q}$
- For diagram d: $\left(\frac{\Lambda}{M^2}\right) \times \left(\frac{M}{Q^2}\right)^3 \times Q^3 \times \frac{Q^2}{M} \times \frac{\alpha}{Q^2} = \frac{\Lambda}{Q}\frac{\alpha}{Q^2} = \mathcal{O}((\mathcal{K})) \times \frac{\alpha M}{Q}$
- For diagram e: $\frac{\alpha}{p^2} = \mathcal{O}(a) \times \frac{Q}{\Lambda}$,

where $\mathcal{O}(\mathcal{K})$ is the contribution from the one nucleon exchange diagram (see Fig. 3):

$$\mathcal{O}(\mathcal{K}) = \frac{\Lambda}{MQ^2}. \tag{37}$$

The above discussion indicates that diagram (e) is of higher order than diagrams a-d, and would not be taken into account at NLO. Diagram (f) is the contribution from the non-perturbative proton-proton propagator which affects the ^{3}H-^{3}He binding energy difference, as discussed in detail in [18], and will be shown later.

3. *The doublet channel*

Like ^{3}H, ^{3}He also has a doublet channel, which can be depicted as a proton and a deuteron whose spins are coupled to a total spin of 1/2. In the intermediate state, a spin-singlet dibaryon can appear, leading to two coupled amplitudes that differ in the type of the outgoing dibaryon, as shown in Fig. 6. In contrast to ^{3}H two different projections for the singlet amplitude: $np(S), pp(P)$, due to the fact that the electromagnetic interaction does not couple to isospin eigenstates [16]. The Faddeev equation for ^{3}He, at LO, can be written as:

$$\begin{aligned} t^{LO}(k,p,E) &= B_0(k,p,E) \\ &+ \left[K_0^{(S)}(q,p,E) + K_0^C(q,p,E)\right] \otimes t^{LO}(k,p,E)\ , \end{aligned} \tag{38}$$

where the amplitude has three components in this case:

$$t^{LO}(k,q,E) = \begin{pmatrix} T^\alpha(k,q,E) \\ S^\alpha(k,q,E) \\ P^\alpha(k,q,E) \end{pmatrix}\ , \tag{39}$$

The α indicates that the ^{3}He nuclear amplitudes (T,S,P) are calculated in the presence of a Coulomb interaction (of strength α).

For ^{3}He we find:

$$B_0 = Q_0\left(\frac{k^2+p^2-ME}{kp}\right)\begin{pmatrix} \frac{y_t^2}{2kp}\left(1+\frac{2H(\Lambda)}{\Lambda^2}\right) \\ \frac{-y_t y_s}{2kp}\left(1+\frac{2H(\Lambda)}{3\Lambda^2}\right) \\ \frac{-y t y s}{kp}\left(1+\frac{2H(\Lambda)}{3\Lambda^2}\right) \end{pmatrix} + \begin{pmatrix} y_t^2\left[K_C^a(k,p)+K_C^b(k,p)\right] \\ y_t y s K_C^c(k,p) \\ -2y_t y s K_C^b(k,p) \end{pmatrix}\ , \tag{40}$$

$$\begin{aligned} K_0^S(q,p) =& MK_1(q,p,E) \times \begin{pmatrix} y_t^2\cdot D_t(E,q) & -3y_t y_s\cdot D_s(E,q) & -3y_t y_s\cdot D_{pp}(E,q) \\ -y_t y_s\cdot D_t(E,q) & -y_s^2\cdot D_s(E,q) & y_s^2\cdot D_{pp}(E,q) \\ -2y_t y_s\cdot D_t(E,q) & 2y_s^2\cdot D_s(E,q) & 0 \end{pmatrix} + \\ & M\frac{H(\Lambda)}{\Lambda^2}\begin{pmatrix} y_t^2\cdot D_t(E,q) & -y_t y_s\cdot D_s(E,q) & -y_t y_s\cdot D_{pp}(E,q) \\ -\frac{1}{3}y_t y_s\cdot D_t(E,q) & -\frac{1}{3}y_s^2\cdot D_s(E,q) & \frac{1}{3}y_s^2\cdot D_{pp}(E,q) \\ -\frac{2}{3}y_t y_s\cdot D_t(E,q) & \frac{1}{3}y_s^2\cdot D_s(E,q) & \frac{2}{3}y_s^2\cdot D_{pp}(E,q) \end{pmatrix}\ , \end{aligned} \tag{41}$$

and

$$K_0^C(q,p) = M \begin{pmatrix} -y_t^2 D_t(E,q)\cdot\left(2K_C^a + K_C^b\right) & 3y_t y_s D_s(E,q)\cdot\left(K_C^b\right) & 3y_t y_s D_{pp}\cdot\left(K_C^c\right) \\ y_t y_s D_t(E,q)\cdot\left(K_C^b\right) & y_s^2 D_s(E,q)\cdot\left(-K_C^a + K_C^b\right) & -y_s^2 D_{pp}\cdot\left(K_C^c\right) \\ 2y_t y_s D_t(E,q)\cdot\left(K_C^d\right) & -2y_s^2 D_s(E,q)\cdot\left(K_C^d\right) & 0 \end{pmatrix} , \tag{42}$$

where the different contributions of the coulomb interaction are given by:

$$K_C^a(q,q') = \frac{M\alpha}{2qq'} Q\left(-\frac{q^2+q'^2+\lambda^2}{2qq'}\right) \left[\frac{\arctan\left(\frac{q+2q'}{\sqrt{3q^2-4ME}}\right) - \arctan\left(\frac{2q+q'}{\sqrt{3q'-4ME}}\right)}{q-q'}\right] , \tag{43}$$

$$K_C^b(q,q') = \frac{M^2\alpha}{4\left(q^2 - ME + qq' + q'^2\right)} Q\left(\frac{q^2+q'^2-ME}{qq'}\right) \times \left[\frac{\arctan\left(\frac{q+2q'}{\sqrt{3q^2-4ME}}\right) - \arctan\left(\frac{2q+q'}{\sqrt{3q'-4ME}}\right)}{q-q'}\right] , \tag{44}$$

$$\begin{aligned} K_C^c(q,q') = K_C^d(q,q') =& \alpha K_1(q,q',E) \times \frac{1}{4\pi(k-p)} \left[\log\left(2ME - 2k^2 + 2kp - 2p^2\right)\right. \\ & - \log\left(-k\sqrt{4ME - 3k^2 + 2kp - 3p^2} + \right. \\ & \left.\left. p\sqrt{4ME - 3k^2 + 2kp - 3p^2} + 2ME - k^2 - p^2\right)\right] , \end{aligned} \tag{45}$$

are the one photon exchange propagators in momentum space, where λ is a small photon mass, introduced to regulate the numerical problem, and extrapolated to zero a-posteriori.

The fully dressed proton-proton propagator is given by [28, 36]:

$$D_{pp} = \mathcal{D}_{pp}(E - \frac{q^2}{2M}, \mathbf{q}) , \tag{46}$$

where in LO Eq. (10):

$$i\mathcal{D}_{pp}^{AB}(q_0,\mathbf{q}) = i\delta^{AB}\frac{4\pi}{My_t^2}\left[\frac{1}{a_p} + 2\kappa\Phi\left(\kappa/q'\right)\right]^{-1} , \tag{47}$$

with

$$\kappa = \frac{\alpha M}{2} , \tag{48}$$

$$q' = i\sqrt{\mathbf{q}^2/4 - Mq_0} , \tag{49}$$

and

$$\Phi(x) = \psi(ix) + \frac{1}{2ix} - \log(ix) , \tag{50}$$

where ψ denotes the logarithmic derivative of the Γ-function.

The experimental data necessary for solving the Faddeev equations with Coulomb interactions are shown in Tab. I.

Parameter	Value	Parameter	Value
γ_t	45.701 MeV [42]	ρ_t	1.765 fm [43]
a_s	-23.714 fm [44]	ρ_s	2.73 fm [44]
a_p	-7.8063 fm [45]	ρ_C	2.794 fm [45]

TABLE I. Experimental two-body parameters used to calculate $A = 3$ nuclei.

E. Limit cycle and three nucleon force.

The above section provides all the necessary information to solve the Faddeev equations for the $p-d$ scattering without cutoff dependence. The three-Body force $H(\Lambda)$ has no isospin dependence, *i.e.* $H(\Lambda)_{^3\mathrm{H}} = H(\Lambda)_{^3\mathrm{He}}$. Using this fact, it is possible to calculate the binding energy of ^{3}He using the three-body force $= H(\Lambda)$ obtained in the triton system. We solve the Faddeev equations for ^{3}He using the three-body force known from ^{3}H at LO with large range of binding energies. The numerical results are shown in Fig. 8. From now on we will use the numerical binding energies $E_{^3\mathrm{He}}(\Lambda)$ at LO as the binding energy of ^{3}He and not $E_{^3\mathrm{He}}$ =7.72 MeV. Therefore, the calculation of the matrix element of the β decay will be performed with those energies, which can lead to some cutoff dependence. We have calculated the Helium-3 energy explicitly using our triton amplitudes and the techniques laid out in Ref. [46].

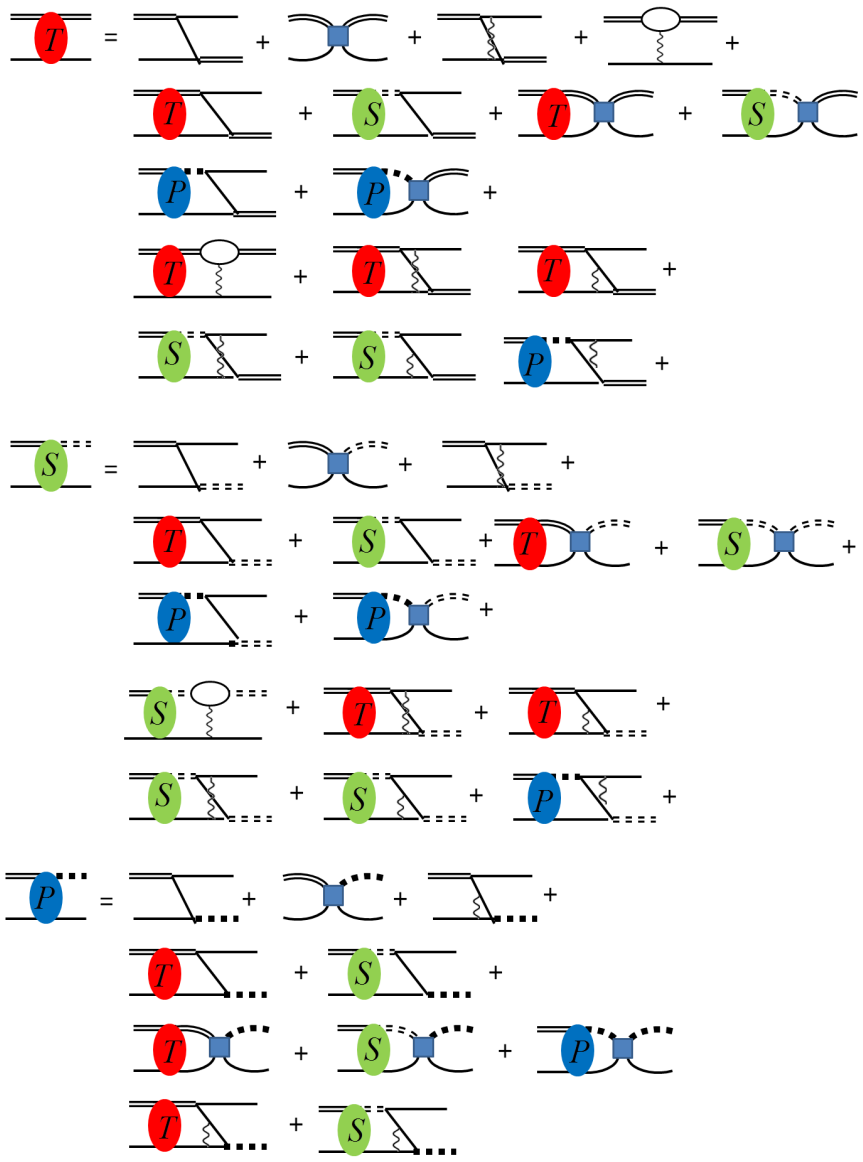

FIG. 6. (Color online) $p-d$ scattering, including a three-body force. The double line denotes the dibaryon propagators D_t (solid) and D_s^{np} (dashed) and D^{pp} (doted). The red bubble (T) represents the triplet channel T=0, S=1, the green bubble (S) represents the singlet channel T=1, S=0 with np dibaryon while the blue bubble (P) represents the singlet channel T=1, S=0 with pp dibaryon.

IV. $A = 3$ MATRIX ELEMENT IN $\not\pi$EFT

In this section we present the general method of calculating an $A = 3$ matrix element in $\not\pi$EFT. This method is used later for calculating the ^{3}He energy shift perturbatively, the NLO contribution for the trinuclei wave functions and tritium β-decay.

A. General $A = 3$ matrix element

The general expression for a reduced matrix element is given by:

$$\langle \mathcal{O}^J \rangle = \frac{\langle I, I_{z_j}, S_j \| \mathcal{L}_{interaction} \| I, I_{z_i}, S_i \rangle}{\sqrt{2J+1}} \tag{51}$$

Where:

- I is the total isospin $=\frac{1}{2}$ for three-nucleons system.
- $I_{z_{i,j}}$ are the initial and final isospin projection, respectively.

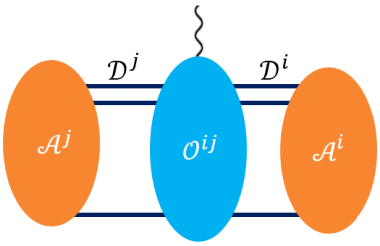

FIG. 7. Diagrammatic representation for matrix elements between three nucleon fields. The LHS of the diagram is final state $\mathcal{A}^j$ while the RHS is initial state $\mathcal{A}^i$. The double line is a propagator of the two intermediate auxiliary fields $\mathcal{D}$.

- $S_{i,j}$ are the initial and final spin projection, respectively.
- J is the operator total spin

The diagrammatic representation of the matrix between three nucleon field is given in Fig. 7. For ^{3}H and ^{3}He in the doublet channel $S_i = S_j = \frac{1}{2}$, eq. (51) can be written as:

$$\langle \mathcal{O}^J \rangle = \frac{\langle I, I_{z_j}, S_j \| \mathcal{L}_{interaction} \| I, I_{z_i}, S_i \rangle}{\sqrt{2J+1}} = \frac{1}{\sqrt{Z_{3,i} Z_{3,j}}} \langle \Gamma_A(q, E_3) | \, f(q,q') \, | \Gamma_B(q', E_3) \rangle \times \times \frac{\left\langle I, I_{z_j}, \frac{1}{2} \middle\| \mathcal{O}^J_{ij} \middle\| I, I_{zi}, \frac{1}{2} \right\rangle}{\sqrt{2J+1}}. \tag{52}$$

Where A, B are the different channels of the three-nucleons homogeneous amplitudes: (T, S) for ^{3}H and (T, S, P) for ^{3}He. $Z_{3,i}$ and $Z_{3,i}$ denote the three-nucleon fields normalizations and $f(q, q')$ is the interaction kernel (as discussed further below) of the weak operator in terms of momenta q, q'.

1. *Constructing the interaction kernel $f(q, q')$*

We construct the interaction kernel $f(q, q')$ using the following Feynman rules:

1. For every single-nucleon line include a factor

$$iS(q)^{\alpha a}_{\beta b} = i\delta^a_b \delta^\alpha_\beta \left[q_0 - \frac{\mathbf{q}^2}{2M} + i\varepsilon \right]^{-1} .$$

2. For every spin-singlet dibaryon vertex-NN vertex insert a factor

$$-2iy_s P_s \ .$$

3. For every spin-triplet dibaryon vertex-NN vertex

$$-2iy_t P_t \ ,$$

where P_t and P_s are given in Eq. (2).

4. For every dibaryon propagator up to NLO include the corresponding propagator introduced in eqs. (6) and (12).

5. For every loop momentum insert the measure

$$\int \frac{\mathrm{d}^4 q}{(2\pi)^4} \ ,$$

perform the q_0-integration using contour integration.

B. Example: ^{3}He-^{3}H binding energy difference with perturbative Coulomb

The energy difference between ^{3}H and ^{3}He can be calculated perturbatively as matrix element of LO one-photon exchange diagrams (Fig. 5 a-d,f), between two triton bubbles, by summing over all diagrams which contribute to the perturbative ^{3}H-^{3}He energy shift [18, 46].

The Coulomb-induced energy shift is defined as:

$$-E_{^3\mathrm{He}} = -E_{^3H} + \Delta E. \tag{53}$$

In terms of eq. (52), ΔE has the form:

$$\Delta E = Z_{^3H}^{-1} \sum_{A,B=t,s} \langle \Gamma_A(q, E_{^3H}) | \, f^C_{AB}(q,q') \, | \Gamma_B(q', E_{^3H}) \rangle \, , \tag{54}$$

where $f^C_{AB}(q, q')$ is the Coulomb-interaction kernel containing one-photon exchange.

The matrix element originates from Fig. 5 a-d is given by:

$$\Delta E = \frac{1}{Z_{^3\mathrm{H}}} \begin{pmatrix} D_t(q,E)\Gamma_T(q,E) \\ D_s(q,E)\Gamma_S(q,E) \end{pmatrix}^T \otimes \begin{pmatrix} y_t^2\left[-2K_C^a(q,q',E)+K_C^b(q,q',E)\right] & 3y_ty_s\left[K_C^b(q,q',E)+K_C^c(q,q',E)\right] \\ y_ty_s\left[2K_C^a(q,q',E)-K_C^b(q,q',E)+3K_C^c(q,q',E)\right] & y_s^2\left[K_C^b(q,q',E)+K_C^d(q,q',E)\right] \end{pmatrix} \otimes \begin{pmatrix} D_t(q,E)\Gamma_T(q,E) \\ D_s(q,E)\Gamma_S(q,E) \end{pmatrix} \quad (55)$$

where $Z^{^3\mathrm{H}}$ is ^{3}H normalization and K_C^a, K_C^b, K_C^c are the Coulomb corrections in momentum space (Fig. . 5).

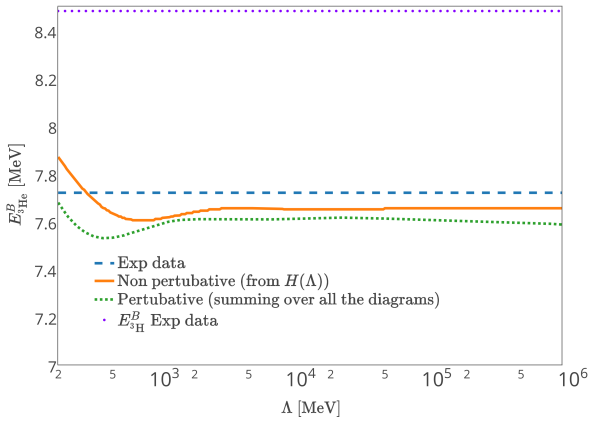

FIG. 8. (Color online) Prediction for the $E_{^3\mathrm{He}}$ binding energy as a function of the cutoff. The solid line is the binding energy from the non perturbative solution (Sub-section III E), the dotted line is the prediction from perturbation theory(eqs. (55) and (56)). The dashed line is the experimental value $E_{^3\mathrm{He}} = 7.72$ MeV.

The energy shift originates from the proton-proton propagator (Fig. 5 (f), see [46] for more details):

$$\Delta E^C = \frac{1}{Z_{^3\mathrm{H}}} \left\langle \Gamma_S\left(q, E^B_{^3\mathrm{H}}\right) \left| f^C_{pp}(q) \right| \Gamma_S\left(q, E^B_{^3\mathrm{H}}\right) \right\rangle . \quad (56)$$

Where:

$$f^C_{pp}(q) = \frac{1}{a_C} - \frac{1}{a_s} + \alpha M \Phi\left(\frac{\alpha M/2}{\sqrt{3q^2/4 - M E^B_{^3\mathrm{H}}}}\right) . \quad (57)$$

Fig. 8 shows that summing over all the possible one photon exchange diagrams is consistent with the non-perturbative results calculated using the methods presented in Sec. III E. These results reproduce the calculations presented in Ref. [17], a fact which serves as a validation of the numerical calculation presented here.

V. PERTURBATIVE CORRECTION TO THE NUCLEAR WAVE FUNCTIONS: $\not\pi$EFT AT NEXT-TO-LEADING ORDER

The ingredients needed for a consistent calculation of triton β-decay up to NLO, are the current operator and the bound state amplitudes up to this order. In this section, we will discuss how we obtain the bound state amplitude at NLO. Specifically, we follow the NLO bound state calculation of Vanasse *et al.* [17, 35].

In our notation, we distinguish between the NLO correction to the t-matrix $t(k,p,E)$ and the NLO correction of the bound state scattering amplitude($\mathcal{B}(k)$) which is the homogeneous solution of the Faddeev equation.

A. The NLO correction to the t-matrix

The full t-matrix can be expanded order by order

$$t(k,p,E) = t^{LO}(k,p,E) + t^{NLO}(k,p,E) + \dots . \quad (58)$$

Where $t^{LO}(k,p,E)$ is given in Eq. (15). The NLO correction to $t(k,p,E)$ contains the effective range correction and an NLO 3-body force $H^{NLO}(\Lambda)$. When the energy E is close to the three-nucleon bound state energy, the amplitude $t^{LO}(k,p,E)$ can be written as

$$t^{LO}(k,p,E) = \frac{\mathcal{B}(k)\mathcal{B}(p)}{E - E_B} . \quad (59)$$

In general $t^{LO}(k,p,E)$ contains additional regular terms which can be neglected due to the energy pole.

Therefore:

$$t(k,p,E) = t^{LO}(k,p,E) + t^{LO}(k,q,E) \otimes M^{NLO}(q,q') \otimes t^{LO}(q',p,E) \quad (60)$$

where $M^{NLO}(q,q')$ are all the NLO corrections to the T-matrix (see Fig. 9). For simplicity, here we write the NLO correction for the case that the T-matrix contains only the triplet channel, *i.e.* $t(k,p,E) = T(k,p,E)$, given

by:

$$
\begin{aligned}
&T(k,p,E)^{NLO} = \\
&\frac{\rho_t}{4\pi}\int_0^\Lambda dqq^2 T^{LO}(k,q,E)\frac{\sqrt{3q^2/4-ME-i\epsilon}+\gamma}{\sqrt{3q^2/4-ME-i\epsilon}-\gamma}\times \\
&\qquad T^{LO}(q,p,E)+ \\
&T^{LO}(k,q,E)\otimes\{K_1(q,q',E)\times \\
&\qquad y_t^2\left[D_t^{NLO}(E,q)-D_t^{LO}(E,q)\right]\}\otimes T^{LO}(q',p,E)+ \\
&\frac{H^{NLO}}{\pi^2\Lambda^2}\left\{\left[\int_0^\Lambda T^{LO}(k,q,E)\delta_t(E,q)q^2dq\right]\times\right. \\
&\left.\left[\int_0^\Lambda T^{LO}(q,p,E)\delta_t(E,q)q^2dq\right]\right\}.
\end{aligned}
\tag{61}
$$

Where ρ_t is the effective range and H^{NLO} is the NLO correction to the three-body force, and K_1 is defined in eq. (20).

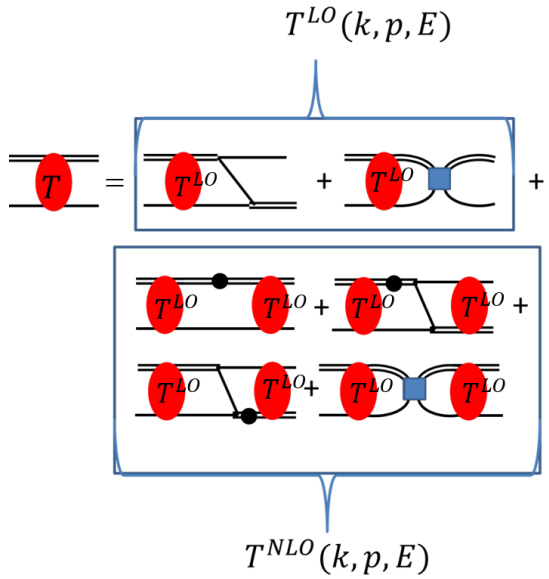

FIG. 9. The Full T-matrix describing a bound state up to NLO. The LO T-matrix is the result of the LO homogeneous Faddeev equation - Eq. (15). The NLO correction to the T-matrix includes both three-body force $H^{NLO}(\Lambda)$ and the effective range ρ.

B. Corrections to the pole position

We would like to use eq. (61) to predict the NLO correction to ^{3}H binding energy. Following Vanasse et al [17], we extend the method used by Ji, Phillips and Platter [47] to include complications due to isospin. At the bound state, the scattering amplitude possesses a pole and can be written (without terms regular at $P_0 = E = -E_B$):

$$
\begin{aligned}
T(k,p,E) =& T^{LO}(k,p,E)+T^{NLO}(k,p,E) = \\
&\frac{Z^{LO}(k,p)+Z^{NLO}(k,p)}{E-(E_B+\Delta E_B)}.
\end{aligned}
\tag{62}
$$

At LO the residue vector function about the pole Z_0 is defined as [47]:

$$
Z_0(k,p) = \lim_{E\to E_B}(E-E_B)T^{LO}(k,p,E), \tag{63}
$$

and ΔE_B is the NLO correction to the binding energy. Keeping ΔE_B to first order in ERE (NLO), one finds that [48]:

$$
\Delta E_B = \lim_{E\to E_B}\frac{(E-E_B)^2T^{NLO}(k,p,E)}{Z_0(k,p)}. \tag{64}
$$

eq. (64) seems to have dependence in the incoming and outgoing momenta (k,p). However, we expect that the NLO binding energy would depend only on cutoff Λ, similarly to LO (as shown in Fig. 8).

Using eq. (59), in bound state, eq. (61) has the form:

$$
\begin{aligned}
&T(k,p,E)^{NLO}(E-E_B)^2 = \\
&\qquad \mathcal{B}(k)^{LO}\mathcal{B}(q)^{LO}\otimes M^{NLO}(q,q')\otimes\mathcal{B}(q')^{LO}\mathcal{B}(p)^{LO}
\end{aligned}
\tag{65}
$$

Since $Z_0(k,p) = lim_{E\to E_B}\mathcal{B}(k)\mathcal{B}(p)$, eq. (64) becomes:

$$
\Delta E_B = \mathcal{B}^{LO}(q)\otimes M^{NLO}(q,q')\otimes\mathcal{B}^{LO}(q') = a(\Lambda) \tag{66}
$$

and:

$$
T^{NLO}(k,p,E) = a(\Lambda)\frac{T^{LO}(k,p,E)}{E-E_B} \tag{67}
$$

From eqs. (61), (63), (64) and (67) we get that:

$$
\Delta E_B = \lim_{E\to E_B}\frac{(E-E_B)^2a(\Lambda)T^{LO}(k,p,E)}{(E-E_B)^2T^{LO}(k,p,E)} = a(\Lambda). \tag{68}
$$

Where for ^{3}H, ΔE_B is set to zero to fix the NLO 3 body force. In the case of ^{3}He we set ΔE_B such:

$$
E = E_B+\Delta E_B = E_B(\Lambda)^{LO}+\Delta E_B = 7.72\text{ MeV}. \tag{69}
$$

For ^{3}He, the following consistency criterion is *a-priori* found:

$$
\frac{\Delta E_B}{E_B} \ll 1 \tag{70}
$$

We return to this in the next subsection.

C. Corrections to the wave function and normalization

(71)

The NLO wave function normalization coefficient is defined as (eq. (62)):

$$Z^{NLO}(k,p,E) = T^{NLO}(k,p,E)(E - E_B - \Delta E_B) \quad (72)$$

For ^{3}H, $\Delta E_B = 0$ in order to set the NLO three-body force (see [17] for more details). In that case:

$$Z^{NLO}(k,p,E) = T^{NLO}(k,p,E)(E - E_B) = \quad (73)$$
$$a(\Lambda)T^{LO}(k,p,E) = \Delta E_B T^{LO}(k,p,E) = 0,$$

i.e. there is a no change of the normalization.

In the case of ^{3}He, the NLO binding energy is set to fit the experimental binding energy - $\Delta E_B \neq 0$. Therefore $Z^{NLO}(k,p,E) \neq 0$ and a NLO description of the scattering amplitude $\mathcal{B}$ is needed.

We note the NLO shift ΔE_B in the binding energy shift is a result of a matrix element whose calculation requires integration over two LO scattering amplitudes - eq. (66) (see Fig. 10).

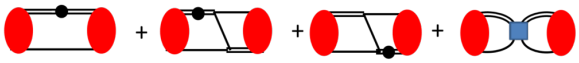

FIG. 10. The diagrammatic form of the NLO correction to binding energy - ΔE_B. The black circle is the effective range insertion while the blue square is the NLO 3-body force.

eq. (66) indicates that for $\Delta E_B = 0$, $M^{NLO}(q,q') \otimes \mathcal{B}(q')^{LO}$ is orthogonal to $\mathcal{B}(q)^{LO}$, where $\mathcal{B}(q)^{LO}$ is the homogeneous solution of:

$$\mathcal{B}(q)^{LO} = M^{LO}(q,q') \otimes \mathcal{B}(q')^{LO}. \quad (74)$$

In similar way one can define:

$$\mathcal{B}(q)^{NLO} = M^{NLO}(q,q') \otimes \mathcal{B}(q'). \quad (75)$$

For $\Delta E_B = 0$:

$$\langle \mathcal{B} | \mathcal{B}^{NLO} \rangle = 0 \quad (76)$$

which is the NLO correction to the scattering amplitude normalization. The full scattering equation for $\mathcal{B}(q)$ is given by:

$$\mathcal{B}(q) = M^{LO}(q,q') \otimes \mathcal{B}(q')^{LO} + M^{NLO}(q,q') \otimes \mathcal{B}^{LO}(q') \quad (77)$$

which is no longer a Bethe-Salpeter equation and therefore the Bethe-Salpeter normalization condition is not valid.

The general form of a NLO matrix element is given by:

$$\mathcal{O}^{LO} + \mathcal{O}^{NLO} = \underbrace{\langle \mathcal{B}^{LO} | \mathcal{O}^{LO} \mathcal{B}^{LO} \rangle}_{\mathcal{O}^{LO}} +$$
$$\underbrace{\langle \mathcal{B}^{LO} | \mathcal{O}^{NLO} | \mathcal{B}^{LO} \rangle + \langle \mathcal{B}^{NLO} | \mathcal{O}^{LO} | \mathcal{B}^{LO} \rangle + \langle \mathcal{B}^{LO} | \mathcal{O}^{LO} | \mathcal{B}^{NLO} \rangle}_{\mathcal{O}^{NLO}} \quad (78)$$

which is shown in Fig. 11.

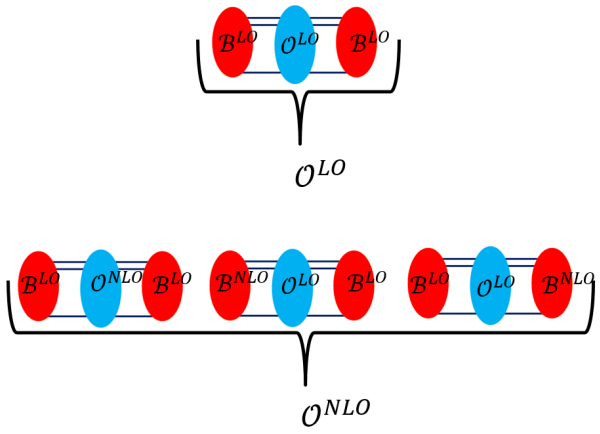

FIG. 11. The diagrammatic form of the full NLO matrix element.

D. The triton channel

1. *The NLO correction to triton homogeneous wave function*

The NLO corrections for triton are constructed from the effective range expansion and from an additional 3-body force. For the remainder of this section, we assume the energy to be close to the triton binding energy. The two components of the T-matrix are therefore given by

$$T(k,p,E) = \frac{\Gamma_T(k,E)\Gamma_T(p,E)}{E - E_B} \quad (79)$$

$$S(k,p,E) = \frac{\Gamma_T(k,E)\Gamma_S(p,E)}{E - E_B} \quad (80)$$

The NLO correction to $T(k,p,E)$ (t-matrix) is given by:

$$\begin{aligned}
T(k,p,E)^{NLO}_{bound}(E-E_B)^2 =& \frac{\rho_t}{4\pi}\int_0^\Lambda dqq^2\Gamma_T(k,E)\Gamma_T(q,E)\frac{\sqrt{3q^2/4-ME-i\epsilon}+\gamma_t}{\sqrt{3q^2/4-ME-i\epsilon}-\gamma_t}\Gamma_T(q,E)\Gamma_T(p,E)+ \\
& \frac{9\rho_s}{8\pi}\int_0^\Lambda dqq^2\Gamma_T(k,E)\Gamma_S(q,E)\frac{3q^2/4-ME-i\epsilon}{\left(\sqrt{3q^2/4-ME-i\epsilon}-\gamma_s\right)^2}\Gamma_S(q,E)\Gamma_T(p,E)+ \\
& \begin{pmatrix}\Gamma_T(k,E)\Gamma_T(q,E)\\ \Gamma_T(k,E)\Gamma_S(q,E)\end{pmatrix}^T\otimes\{-K_1(q,q',E)\times \\
& \begin{pmatrix}-y_t^2\Delta_t(E,q) & 3y_ty_s\Delta_s(E,q)\\ 3y_ty_s\Delta_t(E,q) & -y_s^2\Delta_s(E,q)\end{pmatrix}\}\otimes\begin{pmatrix}\Gamma_T(q',E)\Gamma_T(p,E)\\ \Gamma_S(q',E)\Gamma_T(p,E)\end{pmatrix}+ \\
& \frac{H^{NLO}}{\pi^2\Lambda^2}\left\{\left[\int_0^\Lambda\frac{\Gamma_T(k,E)\Gamma_T(q,E)}{E-E_B}\delta_t(E,q)q^2dq+2\int_0^\Lambda\frac{\Gamma_T(k,E)\Gamma_S(q,E)}{E-E_B}\delta_s(E,q)q^2dq\right]\times\right. \\
& \left.\left[\int_0^\Lambda\Gamma_T(q,E)\Gamma_T(p,E)\delta_t(E,q)q^2dq+2\int_0^\Lambda\Gamma_S(q,E)\Gamma_T(p,E)\delta_s(E,q)q^2dq\right]\right\},
\end{aligned} \tag{81}$$

with:

$$\delta_{t,s}(E,q)=\frac{My_{t,s}^2}{4\pi}D_{t,s}(E,q) \tag{82}$$

and

$$\Delta_{t,s}(E,q)=D^{NLO}_{t,s}(E,q)-D^{LO}_{t,s}(E,q). \tag{83}$$

K_1 is defined in eq. (20), and Γ_T and Γ_S are LO homogeneous solution to the Faddeev equations (eq. (32)).

Similarly for $S(k,p)$:

$$\begin{aligned}
S(k,p)^{NLO}_{bound}(E-E_B)^2 =& \frac{\rho_t}{4\pi}\int_0^\Lambda dqq^2\Gamma_T(k,E)\Gamma_S(q,E)\frac{\sqrt{3q^2/4-ME-i\epsilon}+\gamma_t}{\sqrt{3q^2/4-ME-i\epsilon}-\gamma_t}\Gamma_T(q,E)\Gamma_S(p,E) \\
&+\frac{9\rho_s}{8\pi}\int_0^\Lambda dqq^2\Gamma_T(k,E)\Gamma_S(q,E)\frac{3q^2/4-ME-i\epsilon}{\left(\sqrt{3q^2/4-ME-i\epsilon}-\gamma_s\right)^2}\Gamma_S(q,E)\Gamma_S(p,E) \\
&+\begin{pmatrix}\Gamma_T(k,E)\Gamma_T(q,E)\\ \Gamma_S(k,E)\Gamma_T(q,E)\end{pmatrix}^T\otimes\left[-K_1(q,q',E)\begin{pmatrix}-y_t^2\Delta_t(E,q) & 3y_ty_s\Delta_s(E,q)\\ 3y_ty_s\Delta_t(E,q) & -y_s^2\Delta_s(E,q)\end{pmatrix}\right]\otimes\begin{pmatrix}\Gamma_T(q',E)\Gamma_S(p,E)\\ \Gamma_S(q',E)\Gamma_S(p,E)\end{pmatrix} \\
&+\frac{H^{NLO}}{\pi^2\Lambda^2}\left\{\left[\int_0^\Lambda\frac{\Gamma_T(k,E)\Gamma_T(q,E)}{E-E_B}\delta_t(E,q)q^2dq+2\int_0^\Lambda\frac{\Gamma_T(k,E)\Gamma_S(q,E)}{E-E_B}\delta_s(E,q)q^2dq\right]\times\right. \\
&\left.\left[\int_0^\Lambda\Gamma_T(q,E)\Gamma_T(p,E)\delta_t(E,q)q^2dq+2\int_0^\Lambda\Gamma_S(q,E)\Gamma_T(p,E)\delta_s(E,q)q^2dq\right]\right\}.
\end{aligned} \tag{84}$$

The diagrams describing the NLO correction for homogeneous scattering amplitudes are shown in Fig. 12. From Fig. 12 and eqs. (81) and (84) it is clear that the NLO correction for the bound state has no dependence in k,p, therefore:

$$T(k,p,E)^{NLO}_{bound}=\frac{a(\Lambda)}{(E-E_B)^2}\Gamma_T(k,E)\Gamma_T(p,E), \tag{85}$$

and

$$S(k,p)^{NLO}_{bound}=\frac{a(\Lambda)}{(E-E_B)^2}\Gamma_T(k,E)\Gamma_S(p,E), \tag{86}$$

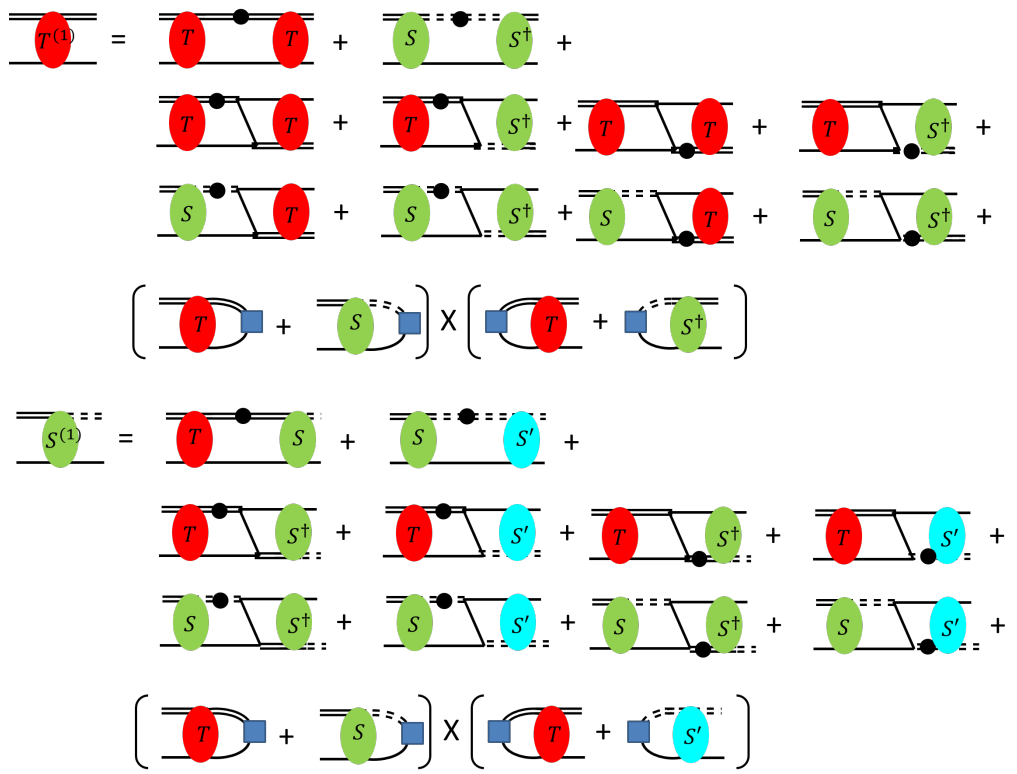

FIG. 12. (Color online) The NLO correction to the ^{3}H t-matrices. The double line is a propagator of the two intermediate auxiliary fields D_t (solid) and D_s^{np} (dashed). The red bubble (T) represents the triplet channel T=0, S=1 ($\Gamma_T(k,E)\Gamma_T(p,E)$), the green bubble (S) represents the singlet channel T=1, S=0 ($(\Gamma_T)(k)\Gamma_S(p)$) while the cyan bubble represents (S') the singlet channel T=1, S=0 ($(\Gamma_S)(k)\Gamma_S(p,E)$). The black circle denotes the NLO correction to dibaryon propagator, while the blue square is the NLO correction to the three-body force ($H^{NLO}(\Lambda)$).

where:

$$
\begin{aligned}
a(\Lambda) = = & \frac{\rho_t}{4\pi}\int_0^\Lambda dq q^2 \Gamma_T^2(q)\frac{\sqrt{3q^2/4-ME-i\epsilon}+\gamma_t}{\sqrt{3q^2/4-ME-i\epsilon}-\gamma_t} + \frac{9\rho_s}{8\pi}\int_0^\Lambda dq q^2\Gamma_S^2(q)\frac{3q^2/4-ME-i\epsilon}{\left(\sqrt{3q^2/4-ME-i\epsilon}-\gamma_s\right)^2} \\
& + \begin{pmatrix}\Gamma_T(q,E)\\ \Gamma_S(q,E)\end{pmatrix}^T \otimes \left[-K_1(q,q',E)\begin{pmatrix}-y_t^2\Delta_t(E,q) & 3y_ty_s\Delta_s(E,q)\\ 3y_ty_s\Delta_t(E,q) & -y_s^2\Delta_s(E,q)\end{pmatrix}\right] \otimes \begin{pmatrix}D_t(q',E)\Gamma_T(q',E)\\ D_s(q',E)\Gamma_S(q',E)\end{pmatrix} \\
& + \frac{H^{NLO}}{\pi^2\Lambda^2}\left[\int_0^\Lambda \Gamma_T(q,E)\delta_t(E,q)q^2dq + 2\int_0^\Lambda \Gamma_S(q,E)\delta_s(E,q)q^2dq\right]^2 .
\end{aligned}
\tag{87}
$$

2. *NLO binding energy and NLO 3-body force*

As mentioned in V B, the NLO correction for the binding energy is given by:

$$\Delta E_B = a(\Lambda) \tag{88}$$

Where for triton, $a(\Lambda)$ is given in eq. (87).

By setting $a(\Lambda)$=0 we find for H^{NLO}:

$$\frac{H^{NLO}[\Lambda]}{\pi^2\Lambda^2} = -\left[\frac{\rho_t}{4\pi}\int_0^\Lambda dq q^2\Gamma_T^2(q)\frac{\sqrt{3q^2/4-ME-i\epsilon}+\gamma_t}{\sqrt{3q^2/4-ME-i\epsilon}-\gamma_t}+\frac{9\rho_s}{8\pi}\int_0^\Lambda dq q^2\Gamma_S^2(q)\frac{3q^2/4-ME-i\epsilon}{\left(\sqrt{3q^2/4-ME-i\epsilon}-\gamma_s\right)^2}+\right.$$
$$\left.\begin{pmatrix}\Gamma_T(q,E)\\ \Gamma_T(q,E)\end{pmatrix}^T\otimes\left\{-K_1(k,q,E)\begin{pmatrix}-y_t^2\Delta_t(E,q) & 3y_ty_s\Delta_s(E,q)\\ 3y_ty_s\Delta_t(E,q) & -y_s^2\Delta_s(E,q)\end{pmatrix}\right\}\otimes\begin{pmatrix}\Gamma_S(p,E)\\ \Gamma_S(q,E)\end{pmatrix}\right]\times$$
$$\left[\int_0^\Lambda\Gamma_T(q,E)\delta_t(E,q)q^2dq+2\int_0^\Lambda\Gamma_S(q,E)\delta_s(E,q)q^2dq\right]^{-2}. \tag{89}$$

The numerical results for $H_{NLO}[\Lambda]$ are shown in Fig. 13. In Fig. 13, we show that we find good agreement with the analytical calculation done by Chen *et al.* [47]. The triton prediction of $H^{NLO}(\Lambda)$ enables us to calculate the NLO corrections to ^{3}He. Similarly to the LO calculation we are using the three-body force to determine the NLO correction to ^{3}He binding energy, by assuming that $H^{NLO}(\Lambda)$ depends on isospin [17].

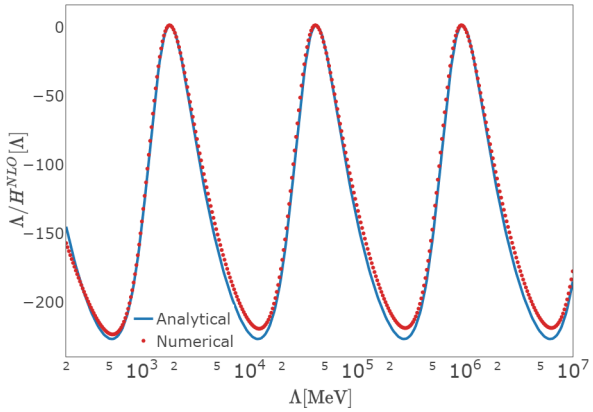

FIG. 13. (Color online) Values of the 3-body force $H(\Lambda)$ in NLO as a function of the cutoff Λ in MeV for ^{3}H. The solid curve shows analytical results for $H(\Lambda)$ from [47], where the dots are the numerical results based on eq. (89).

E. ^{3}He - The NLO correction homogeneous wave function

The equations for the NLO correction to ^{3}He wave functions in bound state are shown in Fig. 14. These equations are similar to those giving the NLO corrections for ^{3}H. However, for ^{3}He there are additional contributions resulting from NLO Coulomb diagrams.

For ^{3}He we have:

$$K_1^S(q,p) = -K_1(q,p,E)\begin{pmatrix}-y_t^2 & 3y_ty_s & 3y_ty_s\\ y_ty_s & y_s^2 & -y_s^2\\ 2y_ty_s & -2y_s^2 & 0\end{pmatrix}\begin{pmatrix}\Delta_t(E,q) & 0 & 0\\ 0 & \Delta_s(E,q) & 0\\ 0 & 0 & \Delta_{pp}(E,q)\end{pmatrix}, \tag{90}$$

and

$$K_1^C(q,p) = M\begin{pmatrix}-y_t^2\left(2K_C^a+K_C^b\right) & 3y_ty_s\left(K_C^b\right) & 3y_ty_s\left(K_C^c\right)\\ y_ty_s\left(K_C^b\right) & y_s^2\left(-K_C^a+K_C^b\right) & -y_s^2\left(K_C^c\right)\\ 2y_ty_s\left(K_C^d\right) & -2y_s^2\left(K_C^d\right) & 0\end{pmatrix}\begin{pmatrix}\Delta_t(E,q) & 0 & 0\\ 0 & \Delta_s(E,q) & 0\\ 0 & 0 & \Delta_{pp}(E,q)\end{pmatrix}, \tag{91}$$

w here K_C^a,K_C^b,K_C^c and K_C^d are defined in Eqs. (43),(44) and (45).

The NLO corrections to ^{3}He amplitudes are given by:

$$
\begin{aligned}
T(k,p,E)^{NLO}_{bound}(E-E_B)^2 = {} & \frac{\rho_t}{4\pi}\int_0^\Lambda dq q^2 \Gamma^\alpha_T(k,E)\Gamma^\alpha_T(q,E)\frac{\sqrt{3q^2/4-ME-i\epsilon}+\gamma_t}{\sqrt{3q^2/4-ME-i\epsilon}-\gamma_t}\Gamma^\alpha_T(q,E)\Gamma^\alpha_T(p,E)+ \\
& \frac{3\rho_s}{4\pi}\int_0^\Lambda dq q^2 \Gamma^\alpha_T(k,E)\Gamma^\alpha_S(q,E)\frac{3q^2/4-ME-i\epsilon}{\left(\sqrt{3q^2/4-ME-i\epsilon}-\gamma_s\right)^2}\Gamma^\alpha_S(q,E)\Gamma^\alpha_T(p,E) \\
& \frac{3\rho_s}{8\pi}\int_0^\Lambda dq q^2 \Gamma^\alpha_T(k,E)\Gamma^\alpha_P(q,E)\frac{3q^2/4-ME-i\epsilon}{\left[2\kappa H\left(\frac{\kappa}{\sqrt{3q^2/4-ME-i\epsilon}}\right)+\frac{1}{a_p}\right]^2}\Gamma^\alpha_P(q,E)\Gamma^\alpha_T(p,E)+ \\
& \begin{pmatrix} \Gamma^\alpha_T(k,E)\Gamma^\alpha_T(q,E) \\ \Gamma^\alpha_T(k,E)\Gamma^\alpha_S(q,E) \\ \Gamma^\alpha_T(k,E)\Gamma^\alpha_P(q,E) \end{pmatrix}^T \otimes \left[K_1^S(q,q',E)+K_1^C(q,q',E)\right] \otimes \begin{pmatrix} \Gamma^\alpha_T(q',E)\Gamma^\alpha_T(p,E) \\ \Gamma^\alpha_S(q',E)\Gamma^\alpha_T(p,E) \\ \Gamma^\alpha_P(q',E)\Gamma^\alpha_T(p,E) \end{pmatrix} + \\
& \frac{H^{NLO}}{\pi^2\Lambda^2}\left\{\left[\int_0^\Lambda \Gamma^\alpha_T(k,E)\Gamma^\alpha_T(q,E)\delta_t(E,q)q^2dq+\int_0^\Lambda \Gamma^\alpha_T(k,E)\Gamma^\alpha_S(q,E)\delta_s(E,q)q^2dq+\right.\right. \\
& \qquad \left.\int_0^\Lambda \Gamma^\alpha_T(k,E)\Gamma^\alpha_P(q,E)\delta_P(E,q)q^2dq\right] \\
& \quad \times\left[\int_0^\Lambda \Gamma^\alpha_T(q,E)\Gamma^\alpha_T(p,E)\delta_t(E,q)q^2dq+\int_0^\Lambda \Gamma^\alpha_S(k,E)\Gamma^\alpha_T(p,E)\delta_s(E,q)q^2dq+\right. \\
& \qquad \left.\left.\int_0^\Lambda \Gamma^\alpha_P(q,E)\Gamma^\alpha_T(p,E)\delta_s(E,q)q^2dq\right]\right\}+ \\
& -\frac{\alpha\rho_t M}{4\pi}\int_0^\Lambda qdq\int_0^\Lambda q'dq'\Gamma^\alpha_T(k,E)\Gamma^\alpha_T(q,E)\delta_t(E,q)Q_0\left(\frac{q^2+q'^2+\lambda^2}{-2qq'}\right)\Gamma^\alpha_T(q',E)\delta_t(q',E)\Gamma^\alpha_T(p,E)+ \\
& -\frac{3\alpha\rho_t M}{4\pi}\int_0^\Lambda qdq\int_0^\Lambda q'dq'\Gamma^\alpha_T(k,E)\Gamma^\alpha_S(q,E)\delta_s(E,q)Q_0\left(\frac{q^2+q'^2+\lambda^2}{-2qq'}\right)\Gamma^\alpha_S(q',E)\delta_s(q',E)\Gamma^\alpha_T(p,E)
\end{aligned}
\tag{92}
$$

$$
\begin{aligned}
S(k,p)^{NLO}_{bound}(E-E_B)^2 = {} & \frac{\rho_t}{4\pi}\int_0^\Lambda dqq^2\Gamma^\alpha_T(k,E)\Gamma^\alpha_T(q,E)\frac{\sqrt{3q^2/4-ME-i\epsilon}+\gamma_t}{\sqrt{3q^2/4-ME-i\epsilon}-\gamma_t}\Gamma^\alpha_T(q,E)\Gamma^\alpha_S(p,E)+ \\
& \frac{3\rho_s}{4\pi}\int_0^\Lambda dqq^2\Gamma^\alpha_T(k,E)\Gamma^\alpha_S(q,E)\frac{3q^2/4-ME-i\epsilon}{\left(\sqrt{3q^2/4-ME-i\epsilon}-\gamma_s\right)^2}\Gamma^\alpha_S(q,E)\Gamma^\alpha_S(p,E) \\
& \frac{3\rho_s}{8\pi}\int_0^\Lambda dqq^2\Gamma^\alpha_T(k,E)\Gamma^\alpha_P(q,E)\frac{3q^2/4-ME-i\epsilon}{\left[2\kappa H\left(\frac{\kappa}{\sqrt{3q^2/4-ME-i\epsilon}}\right)+\frac{1}{a_p}\right]^2}\Gamma^\alpha_P(q,E)\Gamma^\alpha_S(p,E)+ \\
& \begin{pmatrix}\Gamma^\alpha_T(k,E)\Gamma^\alpha_T(q,E)\\ \Gamma^\alpha_T(k,E)\Gamma^\alpha_S(q,E)\\ \Gamma^\alpha_T(k,E)\Gamma^\alpha_P(q,E)\end{pmatrix}^T\otimes\left[K_1^S(q,q',E)+K_1^C(q,q',E)\right]\otimes\begin{pmatrix}\Gamma^\alpha_T(q',E)\Gamma^\alpha_S(p,E)\\ \Gamma^\alpha_S(q',E)\Gamma^\alpha_S(p,E)\\ \Gamma^\alpha_P(q',E)\Gamma^\alpha_S(p,E)\end{pmatrix}+ \\
& \frac{H^{NLO}}{\pi^2\Lambda^2}\Bigg\{\Bigg[\int_0^\Lambda\Gamma^\alpha_T(k,E)\Gamma^\alpha_T(q,E)\delta_t(E,q)q^2dq+\int_0^\Lambda\Gamma^\alpha_T(k,E)\Gamma^\alpha_S(q,E)\delta_s(E,q)q^2dq+ \\
& \qquad\int_0^\Lambda\Gamma^\alpha_T(k,E)\Gamma^\alpha_P(q,E)\delta_P(E,q)q^2dq\Bigg] \\
& \quad\times\Bigg[\int_0^\Lambda\Gamma^\alpha_T(q,E)\Gamma^\alpha_T(p,E)\delta_t(E,q)q^2dq+\int_0^\Lambda\Gamma^\alpha_S(k,E)\Gamma^\alpha_S(p,E)\delta_s(E,q)q^2dq+ \\
& \qquad\int_0^\Lambda\Gamma^\alpha_P(q,E)\Gamma^\alpha_S(p,E)\delta_s(E,q)q^2dq\Bigg]\Bigg\}+ \\
& -\frac{\alpha\rho_t M}{4\pi}\int_0^\Lambda qdq\int_0^\Lambda q'dq'\Gamma^\alpha_T(k,E)\Gamma^\alpha_T(q,E)\delta_t(E,q)Q_0\left(\frac{q^2+q'^2+\lambda^2}{-2qq'}\right)\Gamma^\alpha_T(q',E)\delta_t(q',E)\Gamma^\alpha_S(p,E)+ \\
& -\frac{3\alpha\rho_t M}{4\pi}\int_0^\Lambda qdq\int_0^\Lambda q'dq'\Gamma^\alpha_T(k,E)\Gamma^\alpha_S(q,E)\delta_s(E,q)Q_0\left(\frac{q^2+q'^2+\lambda^2}{-2qq'}\right)\Gamma^\alpha_S(q',E)\delta_s(q',E)\Gamma^\alpha_S(p,E)
\end{aligned}
\tag{93}
$$

$$
\begin{aligned}
P(k,p)^{NLO}_{bound}(E-E_B)^2 = &\frac{\rho_t}{4\pi}\int_0^\Lambda dqq^2\Gamma_T^\alpha(k,E)\Gamma_T^\alpha(q,E)\frac{\sqrt{3q^2/4-ME-i\epsilon}+\gamma_t}{\sqrt{3q^2/4-ME-i\epsilon}-\gamma_t}\Gamma_T^\alpha(q,E)\Gamma_P^\alpha(p,E)+\\
&\frac{3\rho_s}{4\pi}\int_0^\Lambda dqq^2\Gamma_T^\alpha(k,E)\Gamma_S^\alpha(q,E)\frac{3q^2/4-ME-i\epsilon}{\left(\sqrt{3q^2/4-ME-i\epsilon}-\gamma_s\right)^2}\Gamma_S^\alpha(q,E)\Gamma_P^\alpha(p,E)\\
&\frac{3\rho_s}{8\pi}\int_0^\Lambda dqq^2\Gamma_T^\alpha(k,E)\Gamma_P^\alpha(q,E)\frac{3q^2/4-ME-i\epsilon}{\left[2\kappa H\left(\frac{\kappa}{\sqrt{3q^2/4-ME-i\epsilon}}\right)+\frac{1}{a_p}\right]^2}\Gamma_P^\alpha(q,E)\Gamma_P^\alpha(p,E)+\\
&\begin{pmatrix}\Gamma_T^\alpha(k,E)\Gamma_T^\alpha(q,E)\\ \Gamma_T^\alpha(k,E)\Gamma_S^\alpha(q,E)\\ \Gamma_T^\alpha(k,E)\Gamma_P^\alpha(q,E)\end{pmatrix}^T\otimes\left[K_1^S(q,q',E)+K_1^C(q,q',E)\right]\otimes\begin{pmatrix}\Gamma_T^\alpha(q',E)\Gamma_P^\alpha(p,E)\\ \Gamma_S^\alpha(q',E)\Gamma_P^\alpha(p,E)\\ \Gamma_P^\alpha(q',E)\Gamma_P^\alpha(p,E)\end{pmatrix}+\\
&\frac{H^{NLO}}{\pi^2\Lambda^2}\left\{\left[\int_0^\Lambda\Gamma_T^\alpha(k,E)\Gamma_T^\alpha(q,E)\delta_t(E,q)q^2dq+\int_0^\Lambda\Gamma_T^\alpha(k,E)\Gamma_S^\alpha(q,E)\delta_s(E,q)q^2dq+\right.\right.\\
&\qquad\left.\int_0^\Lambda\Gamma_T^\alpha(k,E)\Gamma_P^\alpha(q,E)\delta_p(E,q)q^2dq\right]\times\\
&\qquad\left[\int_0^\Lambda\Gamma_T^\alpha(q,E)\Gamma_P^\alpha(p,E)\delta_t(E,q)q^2dq+\right.\\
&\qquad\left.\left.\int_0^\Lambda\Gamma_S^\alpha(q,E)\Gamma_P^\alpha(p,E)\delta_s(E,q)q^2dq+\int_0^\Lambda\Gamma_P^\alpha(q,E)\Gamma_P^\alpha(p,E)\delta_s(E,q)q^2dq\right]\right\}+\\
&-\frac{\alpha\rho_tM}{4\pi}\int_0^\Lambda qdq\int_0^\Lambda q'dq'\Gamma_T^\alpha(k,E)\Gamma_T^\alpha(q,E)\delta_t(E,q)Q_0\left(\frac{q^2+q'^2+\lambda^2}{-2qq'}\right)\Gamma_T^\alpha(q',E)\delta_t(q',E)\Gamma_T^\alpha(p,E)+\\
&-\frac{3\alpha\rho_tM}{4\pi}\int_0^\Lambda qdq\int_0^\Lambda q'dq'\Gamma_T^\alpha(k,E)\Gamma_S^\alpha(q,E)\delta_s(E,q)Q_0\left(\frac{q^2+q'^2+\lambda^2}{-2qq'}\right)\Gamma_S^\alpha(q',E)\delta_s(q',E)\Gamma_T^\alpha(p,E).
\end{aligned}
\tag{94}
$$

1. NLO binding energy and NLO 3-body force

Similar to the triton, the correction to the binding energy of ^{3}He is $a(\Lambda)$:

$$
\begin{aligned}
\Delta E_B = &\frac{\rho_t}{4\pi}\int_0^\Lambda dqq^2\Gamma_T^\alpha(q,E)\frac{\sqrt{3q^2/4-ME-i\epsilon}+\gamma_t}{\sqrt{3q^2/4-ME-i\epsilon}-\gamma_t}\Gamma_T^\alpha(q,E)+\\
&\frac{3\rho_s}{4\pi}\int_0^\Lambda dqq^2\Gamma_S^\alpha(q,E)\frac{3q^2/4-ME-i\epsilon}{\left(\sqrt{3q^2/4-ME-i\epsilon}-\gamma_s\right)^2}\Gamma_S^\alpha(q,E)\\
&\frac{3\rho_s}{8\pi}\int_0^\Lambda dqq^2\Gamma_P^\alpha(q,E)\frac{3q^2/4-ME-i\epsilon}{\left[2\kappa H\left(\frac{\kappa}{\sqrt{3q^2/4-ME-i\epsilon}}\right)+\frac{1}{a_p}\right]^2}\Gamma_P^\alpha(q,E)+\\
&\begin{pmatrix}\Gamma_T^\alpha(q,E)\\ \Gamma_S^\alpha(q,E)\\ \Gamma_P^\alpha(q,E)\end{pmatrix}^T\otimes\left[K_1^S(q,q',E)+K_1^C(q,q',E)\right]\otimes\begin{pmatrix}D_t(q',E)D_t(q',E)\Gamma_T^\alpha(q',E)\\ D_s(q',E)\Gamma_S^\alpha(q',E)\\ D_{pp}(q',E)\Gamma_S^\alpha(q',E)\end{pmatrix}+\\
&\frac{H^{NLO}}{\pi^2\Lambda^2}\left[\int_0^\Lambda\Gamma_T^\alpha(q,E)\delta_t(E,q)q^2dq+\int_0^\Lambda\Gamma_S^\alpha(q,E)\delta_s(E,q)q^2dq+\int_0^\Lambda\Gamma_S^\alpha(q,E)\delta_s(E,q)q^2dq\right]^2+\\
&-\frac{\alpha\rho_tM}{4\pi}\int_0^\Lambda qdq\int_0^\Lambda q'dq'\Gamma_T^\alpha(q,E)\delta_t(E,q)Q_0\left(\frac{q^2+q'^2+\lambda^2}{-2qq'}\right)\Gamma_T^\alpha(q',E)\delta_t(q',E)\Gamma_T^\alpha(p,E)+\\
&-\frac{3\alpha\rho_tM}{4\pi}\int_0^\Lambda qdq\int_0^\Lambda q'dq'\Gamma_S^\alpha(q,E)\delta_s(E,q)Q_0\left(\frac{q^2+q'^2+\lambda^2}{-2qq'}\right)\Gamma_S^\alpha(q',E)\delta_s(q',E)\Gamma_T^\alpha(p,E).
\end{aligned}
\tag{95}
$$

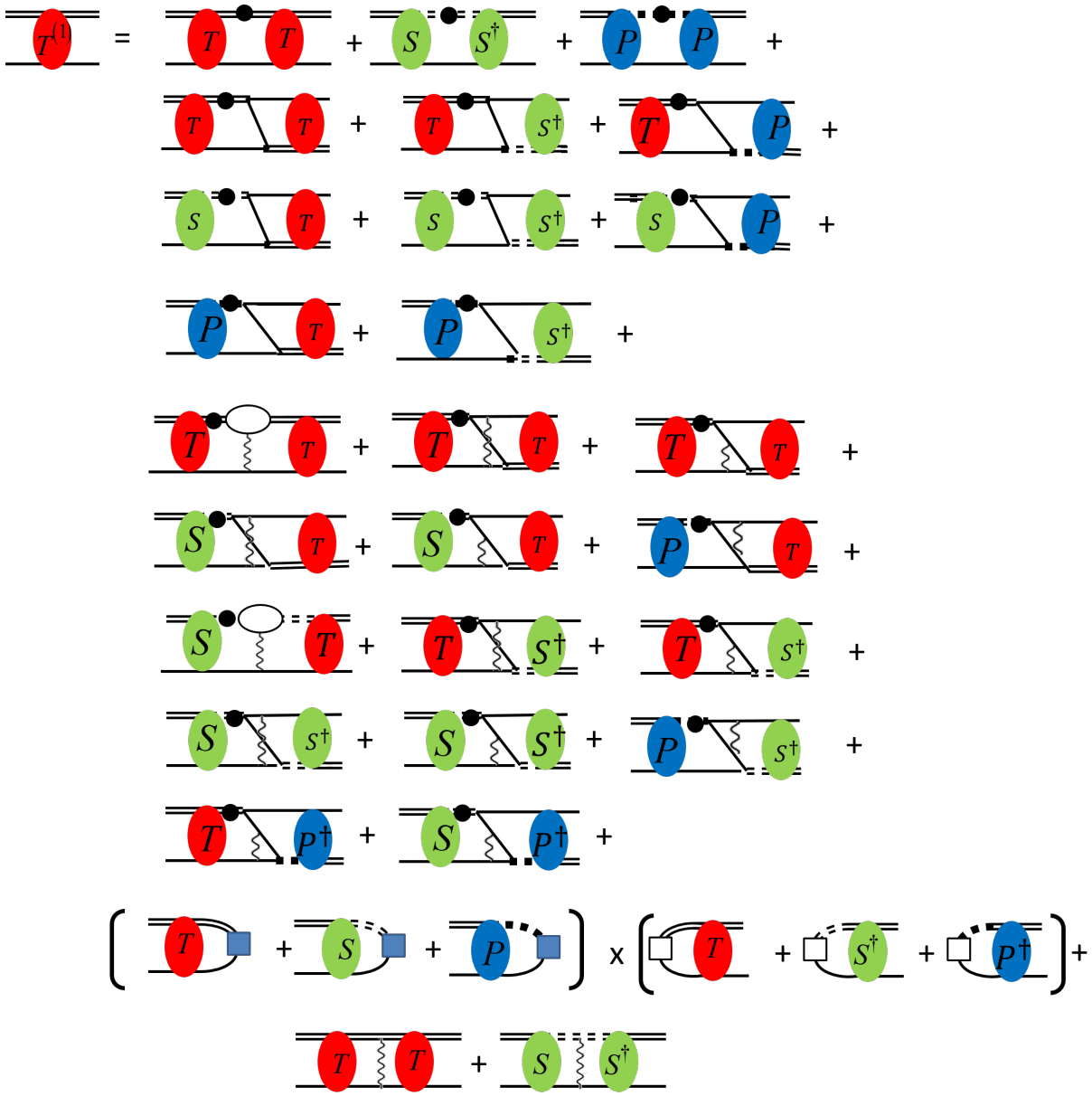

FIG. 14. (Color online) The NLO correction for ^{3}He T-matrices (Shown only for the T channel). The double line is a propagator of the two intermediate auxiliary fields D_t (solid) and D_t^{np} (dashed) and D^{pp} (doted) . The red bubble (T) represents the triplet channel T=0, S=1, the green bubble represents (S) the singlet channel T=1, S=0 with np dibaryon while the blue bubble (P) represents the singlet channel T=1, S=0 with pp dibaryon. The black circle denotes the NLO correction to dibaryon propagator, while the blue square (full) denotes the NLO correction to the three-body force ($H^{NLO}(\Lambda)$).

Where K_1^C and K_1^S are introduce in eqs. (90) and (91) and all the Γ^αs are at LO.

In contrast to triton, here ΔE_B is not zero, due to the fact that H^{NLO} was determined by triton.

ΔE_B diverges with the cutoff Λ (see [17]). To overcome this divergence we define an addition to the three-body force H^α setting $E^{NLO}_{^3\mathrm{He}} = 7.72$, ΔE_B will have Λ dependence:

$$E^{NLO}_{^3\mathrm{He}} = E^{LO}_{^3\mathrm{He}}(\Lambda) + \Delta E_B \tag{96}$$

Where $E^{LO}_{^3\mathrm{He}}(\Lambda)$ is shown in Fig. 8.

$$
\begin{aligned}
H^{\alpha}(\Lambda) = \pi^2\Lambda^2 \Bigg\{ & \frac{7.72 - E^{LO}_{^3\mathrm{He}}(\Lambda)}{\pi^2\Lambda^2} - \frac{\rho_t}{4\pi}\int_0^{\Lambda} dqq^2\Gamma^{\alpha}_T(q,E)\frac{\sqrt{3q^2/4-ME-i\epsilon}+\gamma_t}{\sqrt{3q^2/4-ME-i\epsilon}-\gamma_t}\Gamma^{\alpha}_T(q,E) + \\
& \frac{3\rho_s}{4\pi}\int_0^{\Lambda} dqq^2\Gamma^{\alpha}_S(q,E)\frac{3q^2/4-ME-i\epsilon}{\left(\sqrt{3q^2/4-ME-i\epsilon}-\gamma_s\right)^2}\Gamma^{\alpha}_S(q,E) \\
& \frac{3\rho_s}{8\pi}\int_0^{\Lambda} dqq^2\Gamma^{\alpha}_P(q,E)\frac{3q^2/4-ME-i\epsilon}{\left[2\kappa H\left(\frac{\kappa}{\sqrt{3q^2/4-ME-i\epsilon}}\right)+\frac{1}{a_p}\right]^2}\Gamma^{\alpha}_P(q,E) + \\
& -\frac{\alpha\rho_t M}{4\pi}\int_0^{\Lambda} qdq\int_0^{\Lambda} q'dq'\Gamma^{\alpha}_T(q,E)\delta_t(E,q)Q_0\left(\frac{q^2+q'^2+\lambda^2}{-2qq'}\right)\Gamma^{\alpha}_T(q',E)\delta_t(q',E)\Gamma^{\alpha}_T(p,E) + \\
& \begin{pmatrix}\Gamma^{\alpha}_T(q,E)\\ \Gamma^{\alpha}_S(q,E)\\ \Gamma^{\alpha}_P(q,E)\end{pmatrix}^T \otimes \left[K_1^S(q,q',E)+K_1^C(q,q',E)\right] \otimes \begin{pmatrix} D_t(q',E)\Gamma^{\alpha}_T(q',E)\\ D_s(q',E)\Gamma^{\alpha}_S(q',E)\\ D_{pp}(q',E)\Gamma^{\alpha}_P(q',E)\end{pmatrix} + \\
& -\frac{3\alpha\rho_t M}{4\pi}\int_0^{\Lambda} qdq\int_0^{\Lambda} q'dq'\Gamma^{\alpha}_S(q,E)\delta_s(E,q)Q_0\left(\frac{q^2+q'^2+\lambda^2}{-2qq'}\right)\Gamma^{\alpha}_S(q',E)\delta_s(q',E)\Gamma^{\alpha}_T(p,E)\Bigg\} \times \\
& \left[\int_0^{\Lambda}\Gamma^{\alpha}_T(q,E)\delta_t(E,q)q^2dq + \int_0^{\Lambda}\Gamma^{\alpha}_S(q,E)\delta_s(E,q)q^2dq + \int_0^{\Lambda}\Gamma^{\alpha}_S(q,E)\delta_s(E,q)q^2dq\right]^{-2} - H^{NLO}(\Lambda).
\end{aligned}
\tag{97}
$$

Analytical form of H^{α} are given in [17, 47].

VI. ^{3}H BETA DECAY:

In this section we outline the calculation of the matrix element of the weak reaction:

$$
{}^3\mathrm{H} \rightarrow {}^3\mathrm{He} + e^- + \overline{\nu_e}. \tag{98}
$$

To do so, we make use of the LO and NLO bound state amplitudes for ^{3}H and ^{3}He, calculated in the previous sections. In addition to this, it is essential to define the weak interaction in the $\not\pi$EFT .

A. Weak Interaction in $\not\pi$EFT

The Lagrangian of the weak interaction is given by:

$$
\mathcal{L}_{\mathrm{Weak}} = \frac{-G_F}{\sqrt{2}} l^{\mu}_{+} j^{-}_{\mu} + \mathrm{h.c}\ , \tag{99}
$$

where l^{μ} denotes the leptonic current and J_{μ} the hadronic current.

The hadronic current contains two parts, with polar-vector and axial-vector symmetries $J_{\mu} = V_{\mu} - A_{\mu}$. The part of the polar vector current relevant to β-decay of vanishing energy transfer is,

$$
V_0^- = N^{\dagger}\frac{\tau^-}{2}N. \tag{100}
$$

Here, we utilized the fact that the Conserved Vector Current (CVC) hypothesis is accurate at this order of EFT. The axial-vector part is

$$
\begin{aligned}
\boldsymbol{A}^- = & \frac{g_A}{2}N^{\dagger}\boldsymbol{\sigma}\tau^- N + g_A\left[\frac{1}{2}\frac{\rho_t+\rho_s}{\sqrt{\rho_t\rho_s}} - \right. \\
& \left. L_{1A}\frac{1}{2\pi\sqrt{\rho_t\rho_s}g_A}\left(\mu-\frac{1}{a_t}\right)\left(\mu-\frac{1}{a_s}\right)\right]\left(t^{\dagger}s + s^{\dagger}t\right),
\end{aligned}
\tag{101}
$$

where τ^- is $\tau_1 - i\tau_2$ and g_A and L_{1A} are LECs for weak interaction for one and two-body currents, respectively. In $A = 2$ calculations, the renormalization scale μ is taken arbitrarily, usually at m_{π}. In the current case, a natural choice, which we take, is to set $\mu = \lambda$. One expects that by taking $\lambda \to \infty$ numerically, regularization effects from the treatment of the $A = 3$ system vanish. This entails an asymptotic behavior of L_{1A} which cancels the cutoff dependence in the last term, leaving it RG invariant. Testing this is part of the validation process of our numerical calculation. As a result:

$$
\begin{aligned}
\boldsymbol{A}^- = & \frac{g_A}{2}N^{\dagger}\boldsymbol{\sigma}\tau^- N + g_A\left[\frac{1}{2}\frac{\rho_t+\rho_s}{\sqrt{\rho_t\rho_s}} - \right. \\
& \left. L_{1A}\frac{1}{2\pi\sqrt{\rho_t\rho_s}g_A}\left(\Lambda-\frac{1}{a_t}\right)\left(\Lambda-\frac{1}{a_s}\right)\right]\left(t^{\dagger}s + s^{\dagger}t\right).
\end{aligned}
\tag{102}
$$

$\mathbf{A}^-$ (eq. (102)) is written up to NLO. To maintain consistency, the LO interaction is coupled to the NLO bound state amplitudes (Γs) and to the NLO propagators, while the NLO interactions are coupled to the LO bound state amplitude and to the LO propagators.

B. ^{3}H β-decay matrix elements

The half-life of ^{3}H β-decay can be expressed as [20]:

$$fT_{1/2} = \frac{K/G_V}{\langle F\rangle^2 + \frac{f_A}{f_V} g_A^2 \langle GT\rangle^2} \ ; \tag{103}$$

where $(fT_{1/2})_t = 1129.6 \pm 3$ s [49] is the triton half-life, $K = 2\pi^3 \log 2/m_e^5$ (with m_e denoting the electron mass), G_V is the weak interaction vector coupling constant (such that $K/G_V^2 = 6146.66 \pm 0.6$ [50]), $f_V = 2.8355 \times 10^{-6}$ and $f_A = 2.8506 \times 10^{-6}$ are the Fermi functions calculated by Towner, as reported by Simpson in [51]. In addition,

$$\langle GT\rangle = \frac{\langle ^3\mathrm{He}\|\boldsymbol{A}^-\|^3\mathrm{H}\rangle}{\sqrt{2J+1}} \tag{104}$$

denotes the Gamow-Teller transition, and

$$\langle F\rangle = \frac{\langle ^3\mathrm{He}\|V_0^-|^3\mathrm{H}\rangle}{\sqrt{2J+1}} \tag{105}$$

is the Fermi transition.

The general diagrammatic form of β-decay is shown in Fig. 7. For the weak transitions the left hand side bubble of the diagram is ^{3}H (represented by $\Gamma_{T,S}(q, E_{^3\mathrm{H}})$), while the right hand side bubble is the ^{3}He (represented by $\Gamma^{\alpha}_{T,S,P}(q, E_{^3\mathrm{He}})$).

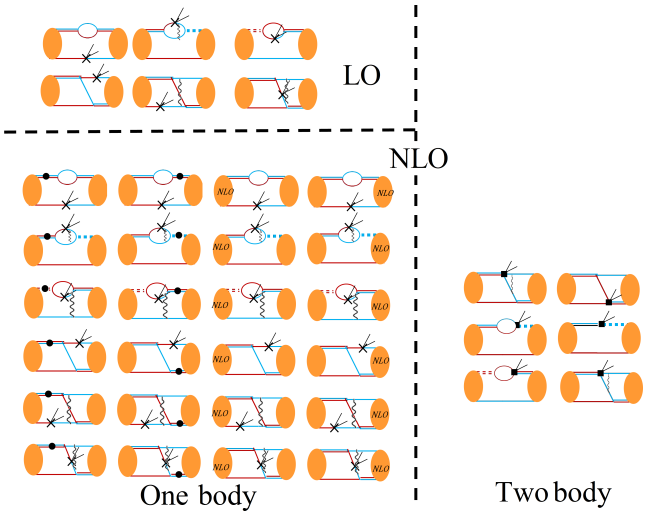

FIG. 15. (Color online) Different topologies of the diagrams contributing to the triton β-decay amplitude. The LHS of each diagram is ^{3}H while the RHS is ^{3}He. The double line is a propagator of the two intermediate auxiliary fields D_t (solid), D_s (dashed for nn and np , dotted for pp), where the red line is the neutron and the blue line is the proton. Most of the diagrams couple both the triplet and the singlet channels. The diagrams with one-body interactions are coupled to g_A while the two-body interaction are coupled to ERE and L_{1A}.

The diagrammatic calculation of $\langle F\rangle$ and $\langle GT\rangle$ transitions is shown in Fig. 15. The LO diagrams contain a one-body weak interaction. These diagrams contribute both to $\langle F\rangle$ and $\langle GT\rangle$ transition. The NLO diagrams contain the NLO corrections for the one-body diagrams, a two-body term originating in ERE, and a two-body weak interaction that is coupled to the unknown universal coupling constant L_{1A}. The two-body diagrams contribute only to $\langle GT\rangle$ transition.

C. Fermi operator

The Fermi transition is defined as:

$$\begin{aligned}\langle F\rangle =& \frac{\langle ^3\mathrm{He}\|V_0^-\|^3\mathrm{H}\rangle}{\sqrt{2J+1}} \\ =& \sqrt{Z_{^3\mathrm{He}} Z_{^3\mathrm{H}}}^{-1} \delta^{S_j}_{S_i} \\ &\times \langle \Gamma_A(q, E_{^3\mathrm{He}})|\, f(q,q')\, |\Gamma_B(q', E_{^3\mathrm{H}})\rangle \ ,\end{aligned} \tag{106}$$

where $Z_{^3\mathrm{He}}$ and $Z_{^3\mathrm{H}}$ are the normalization of the trinucleon homogeneous wave functions. A, B denote the different channels of the 3-nucleons homogeneous scattering amplitude; $A = (T, S, P), B = (T, S)$ and $f(q, q')$ is interaction in terms of momenta q, q'.

We assume momentum conservation for the case of weak transitions, therefore for the Fermi transition:

1. For every one body interaction insert a factor:

$$g_A \delta(q - q')\delta(q_0 - (q_0' - l_0))\frac{2\pi^2}{q^2}$$

Where l_0 is $|E_{^3\mathrm{H}} - E_{^3\mathrm{He}}|$, the energy difference in the weak decay and the q_0-integration is performed using contour integration.

Using the above with the Feynman rules presented in section IV A 1 one finds:

1. For every one body weak interaction containing a bubble insert a factor :

$$\begin{aligned} &f(q,q') \\ &= y_A y_B \frac{4\pi q'^2 \delta(q-q') M^2}{2\pi\left(\sqrt{3q^2 - 4M(E_{^3\mathrm{H}} + l_0)} + \sqrt{3q^2 - 4M E_{^3\mathrm{H}}}\right)}\end{aligned}$$

2. For every weak interaction containing one nucleon exchange:

$$\begin{aligned} f(q,q') =& \frac{M y_A y_B}{2\pi^4 l_0} \times \\ &\log\left[\left(\frac{-E_{^3\mathrm{H}} M + q'^2 - q'q + q^2}{-E_{^3\mathrm{H}} M + q'^2 + q'q + q^2}\right) \times \right. \\ &\left. \left(\frac{-M(E_{^3\mathrm{H}} + l_0) + q'^2 + q'q + q^2}{-M(E_{^3\mathrm{H}} + l_0) + q'^2 - q'q + q^2}\right)\right]\end{aligned}$$

Notice that for $l_0 = 0$, those insertions are reduced to eqs. (29) and (30).

1. Fermi operator without Coulomb.

In the absence of Coulomb, ^{3}H is identical to ^{3}He and the Fermi transition is the triton wave function normalization and therefore:

$$\begin{aligned}\langle F\rangle_{\alpha=0} &= Z_{^3\mathrm{H}}^{-1}\left\langle \Gamma_A(q,E_{^3\mathrm{He}})\right| f(q,q')\left|\Gamma_B(q,E_{^3\mathrm{H}})\right\rangle \delta_{S_i}^{S_j}\\ &= 1\end{aligned} \tag{107}$$

The diagrammatic form of the Fermi using eqs. (29)

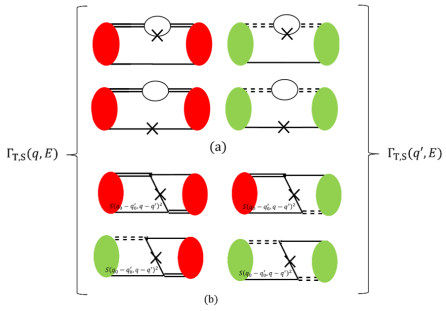

FIG. 16. The diagrammatic form of the LO Fermi transition with $\alpha = 0$. The double line is a propagator of the two intermediate auxiliary fields D_t (solid) and D_s^{np} (dashed). The red bubble (T) represents the triplet channel T=0, S=1, the green bubble (S) represents the singlet channel T=1, S=0 with np dibaryon.

and (30):

$$\begin{aligned}&\left(Z^{^3\mathrm{H}}\right)^{-1} = \left(\hat{\mathcal{D}}\vec{\mathcal{B}}\right)^T \otimes \frac{d}{dE}\left(\hat{I}-K\right)\Big|_{E=-E_B} \otimes \left(\hat{\mathcal{D}}\vec{\mathcal{B}}\right) =\\ &\sum_{A=t,s}\int\frac{d^3q'}{2\pi^3}\int\frac{d^3q}{2\pi^3}\Gamma_A(q,E_{^3\mathrm{H}})D_A(E_{^3\mathrm{H}},q)y_A^2\times\\ &\frac{4\pi q'^2\delta(q-q')M^2}{4\pi\sqrt{3q^2-4ME_{^3\mathrm{H}}}}D_A(E_{q',^3\mathrm{H}}+l)\Gamma_A(q',E_{^3\mathrm{H}})+\\ &\sum_{A=t,s}\int\frac{d^3q'}{2\pi^3}\int\frac{d^3q}{2\pi^3}\Gamma_A(q,E_{^3\mathrm{H}})D_A(E_{^3\mathrm{H}},q)y_A^2\times\\ &\frac{Mq'q}{q^2\left(q'^2-2ME\right)+\left(q'^2-ME\right)^2+q^4}D_A(q,'E_{^3\mathrm{H}})\Gamma_A(q',E_{^3\mathrm{H}})\\ &-6\int\frac{d^3q'}{2\pi^3}\int\frac{d^3q}{2\pi^3}\Gamma_t(q,E_{^3\mathrm{H}})D_t(E_{^3\mathrm{H}},q)y_ty_s\times\\ &\frac{Mq'q}{q^2\left(q'^2-2ME\right)+\left(q'^2-ME\right)^2+q^4}D_s(q,'E_{^3\mathrm{H}})\Gamma_s(q',E_{^3\mathrm{H}})\end{aligned} \tag{108}$$

2. Fermi operator with $\alpha \neq 0$

For the diagrams shown in Fig. 16 (a):

$$\begin{aligned}\langle F\rangle_a &= \sum_{A=t,s}\left\langle \Gamma_A^\alpha(q,E_{^3\mathrm{He}})\right| f(q,q')\left|\Gamma_A(q,E_{^3\mathrm{H}})\right\rangle\\ &= \int\frac{d^3q'}{2\pi^3}\int\frac{d^3q}{2\pi^3}\Gamma_A^\alpha(q,E_{^3\mathrm{H}})D_A(E_{^3\mathrm{H}},q)y_A^2\\ &\times\frac{4\pi q'^2\delta(q-q')M^2}{2\pi\left(\sqrt{3q^2-4M(E_{^3\mathrm{H}}+l_0)}+\sqrt{3q^2-4ME_{^3\mathrm{H}}}\right)}\\ &\times D_A(E_{^3\mathrm{H}}+l_0,q')\Gamma_A^\alpha(q',E_{^3\mathrm{H}}+l_0)\end{aligned} \tag{109}$$

For the diagrams sketched in Fig. 16 (b):

$$\begin{aligned}\langle F\rangle_b &= \sum_{A,B=t,s}\left\langle \Gamma_A^\alpha(q,E_{^3\mathrm{He}})\right| f(q,q')\left|\Gamma_B(q,E_{^3\mathrm{H}})\right\rangle\\ &= \sum_{A,B=t,s}\left[4\delta_B^A-3\right]\times\int\frac{d^3q'}{2\pi^3}\int\frac{d^3q}{2\pi^3}\Gamma_B(q,E_{^3\mathrm{H}})D_B(E_{^3\mathrm{H}},q)\\ &\times\frac{My_Ay_B}{2\pi^4l_0}\left[\log\left(\frac{-E_{^3\mathrm{H}}M+q'^2-q'q+q^2}{-E_{^3\mathrm{H}}M+q'^2+q'q+q^2}\right)\right.\\ &\left.+\log\left(\frac{-M(E_{^3\mathrm{H}}+l_0)+q'^2-q'q+q^2}{-M(E_{^3\mathrm{H}}+l_0)+q'^2+q'q+q^2}\right)\right]\\ &\times\Gamma_A^\alpha(q',E_{^3\mathrm{H}}+l_0)D_A(E_{^3\mathrm{H}}+l_0,q').\end{aligned} \tag{110}$$

Note, that if one sets $\alpha = 0$, and $l_0 = 0$, Eqs. (109) and (110) are reduced to Eq. (108).

Adding Coulomb effects gradually, one can keep $\alpha = 0$, but add isospin breaking in the scattering lengths, *i.e.*, set the physical values for the scattering lengths with $a_{np} \neq a_{pp}$. This calculation enables an isolation of the effect of different scattering lengths to the Fermi transition. To do so we have solved the Faddeev equations for ^{3}He without the one photon exchange (38), with $K_0^C = 0$.

The final step is to calculate the full NLO Fermi transition with $\alpha \neq 0$, using all the diagrams in the left side of Fig. 15.

We have used the experimental data shown in Tab. I as input in our numerical calculation.

The results are shown in Fig. 17 and in Tab. II.

	$\langle F\rangle$
1-body LO $\alpha = 0$	1
1-body LO $\alpha = 0, a_{np} \neq a_{pp}$	0.993
Full NLO	0.9985
SNPA [20]	0.9993

TABLE II. Numerical calculation for $\langle F\rangle$. Note that the second entry is without explicit Coulomb force ($\alpha = 0$), but with isospin breaking in the scattering lengths, *i.e.*, physical values for the scattering lengths $a_{np} \neq a_{pp}$.

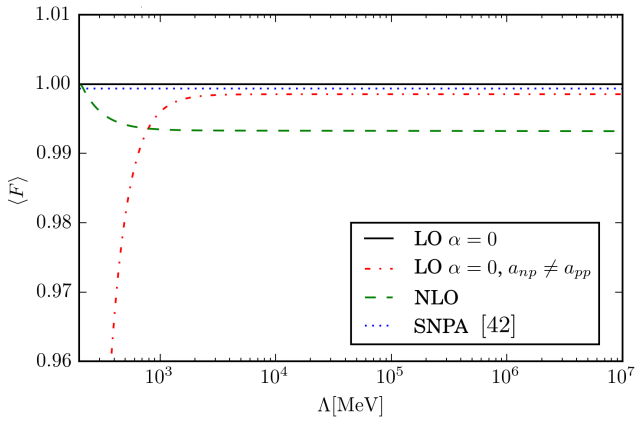

FIG. 17. (Color online) Numerical results for Fermi transition. The solid line is the LO $\langle F\rangle$ with $\alpha = 0$ (1). The dashed-dotted line in the numerical result for $\alpha = 0$ with isospin breaking effects in the scattering lengths $a_{np} \neq a_{pp}$ (LO). The dashed line is the full numerical results up to NLO with $\alpha \neq 0$. The dotted line the value of $\langle F\rangle$ from [20].

Our results compare well to the $\langle F\rangle$ standard nuclear physics approach (SNPA) calculation by Schiavilla *et al.* [20]. The SNPA involves nuclear wave functions derived from high-precision phenomenological nuclear potentials, and one-nucleon and two-nucleon electroweak currents. Clearly, $\langle F\rangle$ is not an observable and can vary between models.

D. Gamow-Teller operator:

1. $\langle GT\rangle$ calculation

In contrast to the Fermi transition, the Gamow-Teller transition involves also two-body operators at NLO.

We denote the various terms in the calculation of the Gamow-Teller transition matrix element with

$$\langle GT\rangle_{LO} = \frac{\langle {}^3\mathrm{He}^{\mathrm{LO}}\|(\boldsymbol{A}^-)^{1-body}\|{}^3\mathrm{H}^{\mathrm{LO}}\rangle}{\sqrt{2J+1}}\ , \tag{111}$$

$$\langle GT\rangle_{NLO} = \frac{\langle {}^3\mathrm{He}^{\mathrm{NLO}}\|(\boldsymbol{A}^-)^{1-body}\|{}^3\mathrm{H}^{\mathrm{LO}}\rangle}{\sqrt{2J+1}} + \frac{\langle {}^3\mathrm{He}^{\mathrm{LO}}\|(\boldsymbol{A}^-)^{1-body}\|{}^3\mathrm{H}^{\mathrm{NLO}}\rangle}{\sqrt{2J+1}}\ , \tag{112}$$

$$\langle GT\rangle_{ERE} = \frac{\langle {}^3\mathrm{He}^{\mathrm{LO}}\|(\boldsymbol{A}^-)^{ERE}\|{}^3\mathrm{H}^{\mathrm{LO}}\rangle}{\sqrt{2J+1}}\ , \tag{113}$$

$$\langle GT\rangle_{L_{1A}} = \frac{\langle {}^3\mathrm{He}^{\mathrm{LO}}\|(\boldsymbol{A}^-)^{L_{1A}}\|{}^3\mathrm{H}^{\mathrm{LO}}\rangle}{\sqrt{2J+1}} \tag{114}$$

Where $(\boldsymbol{A}^-)^{ERE}$ is the term coupled to $\frac{\rho_t+\rho_s}{\sqrt{\rho_t\rho_s}}$ in eq. (102) and $(\boldsymbol{A}^-)^{L_{1A}}$ is the term coupled to L_{1A} in eq. (102).

2. The Gamow-Teller transition at LO

$\langle GT\rangle_{LO}$ originates from the first term in Eq. (101):

$$\frac{g_A}{2} N^\dagger \boldsymbol{\sigma}\tau^- N. \tag{115}$$

The diagrams involving this operator at LO are shown in upper left side of Fig. 15.

The Leading order ^{3}H and ^{3}He amplitudes are given by:

$${}^3\mathrm{H}^{LO} = \begin{pmatrix} \Gamma_T(q, E_{^3\mathrm{H}})^{LO} \cdot D_t^{LO}(E_{^3\mathrm{H}}, q) \\ \Gamma_S(q, E_{^3\mathrm{H}})^{LO} \cdot D_s^{LO}(E_{^3\mathrm{H}}, q) \end{pmatrix} \tag{116}$$

$${}^3\mathrm{He}^{\mathrm{LO}} = \begin{pmatrix} \Gamma_T^\alpha(q, E_{^3\mathrm{He}})^{LO} \cdot \mathcal{D}_t^{LO}(E_{^3\mathrm{He}}, q) \\ \Gamma_S^\alpha(q, E_{^3\mathrm{He}})^{LO} \cdot D_s^{LO}(E_{^3\mathrm{He}}, q) \\ \Gamma_P^\alpha(q, E_{^3\mathrm{He}})^{LO} \cdot D_{pp}^{LO}(E_{^3\mathrm{He}}, q) \end{pmatrix} \tag{117}$$

see Eqs.(26) and (31).

3. One-body operators at NLO

The matrix element $\langle GT\rangle_{NLO}$ originates from the first term of Eq. (101):

$$\frac{g_A}{2} N^\dagger \boldsymbol{\sigma}\tau^- N\ , \tag{118}$$

where in this case either three-body amplitude or the two-body propagator are at NLO. The relevant diagrams are shown in the lower left side of Fig. 15.

For example the NLO vertex: $[\Gamma_T(q, E_B) \cdot D_t(E_B, q)]$ for the triplet channel is given by both the NLO dibaryon propagator (eq. (6)) and the NLO wavefunction (eq. (77)):

$$\begin{aligned} &\Gamma_T(q, E_B)^{NLO} \cdot D_t^{LO}(E_B, q) + \\ &\Gamma_T(q, E_B)^{LO} \cdot D_t^{NLO}(E_B, q)\,. \end{aligned} \tag{119}$$

4. Two-body operators at NLO

The two-body NLO contribution to the GT-transition matrix element originates from the effective range operator that is coupled to g_A:

$$(\boldsymbol{A}^-)^{ERE} = \frac{1}{2}\frac{\rho_t+\rho_s}{\sqrt{\rho_t\rho_s}} g_A \left(t^\dagger s + s^\dagger t\right). \tag{120}$$

In addition there is a two-body NLO weak counterterm with a LEC - L_{1A}:

$$(\boldsymbol{A}^-)^{L_{1A}} = L_{1A}\frac{1}{2\pi\sqrt{\rho_t\rho_s}}\left(\mu - \frac{1}{a_t}\right)\left(\mu - \frac{1}{a_s}\right)\left(t^\dagger s + s^\dagger t\right). \tag{121}$$

The relevant diagrams are shown on the RHS of Fig. 15.

5. $\alpha = 0$

As mentioned before, the matrix element of the Fermi transition at LO between ^{3}H and ^{3}H is 1 (*i.e.* $\alpha = 0$). Similarly, we can calculate the matrix of the Gamow-Teller transition with $\alpha = 0$. By definition:

$$\langle GT\rangle^{LO}_{\alpha=0} = \frac{\langle {}^3\mathrm{H}\|\boldsymbol{\sigma}\|{}^3\mathrm{H}\rangle}{\sqrt{2J+1}} = \sqrt{3}. \tag{122}$$

The NLO contributions to $\langle GT\rangle$ comes from the one-body NLO matrix elements and from the two-body matrix elements. These matrix elements are negative and their summation results in $\langle GT\rangle^{NLO}_{\alpha=0} < \sqrt{3}$. We have performed this calculation in two ways; one where $\alpha = 0$ for both the scattering amplitude and the matrix element, and second where $\alpha = 0$ for the matrix element, but for different scattering lengths, similar to the Fermi case.

VII. NUMERICAL RESULTS FOR GT STRENGTH OF TRITON DECAY

Our numerical results are shown Tab. III and in Fig. 18. We have used the experimental input parameters shown in Tab. I. The full NLO result with $L_{1A} = 0$ includes both one-body and two-body term which contribute to $\langle GT\rangle$, without the diagrams that are coupled to L_{1A}.

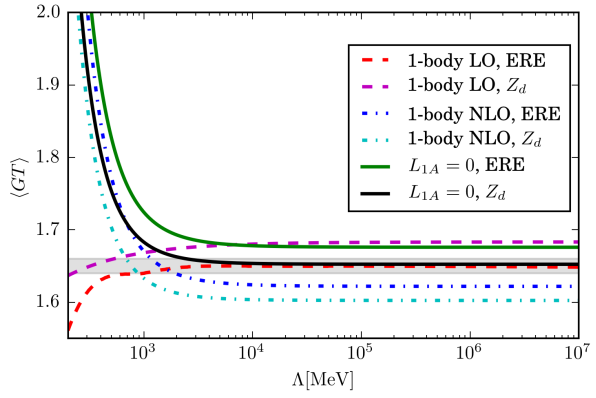

FIG. 18. (Color online) Numerical results of Gamow-Teller transition. The grey area is the full $\langle GT\rangle$ with $g_A = 1.273 \pm 0.003 \pm 0.005$ [52, 53]. The short dashed lines are the numerical results of $\langle GT\rangle_{LO}$, the dashed-dotted lines are the numerical results of one body- $\langle GT\rangle_{NLO}$, the solid lines show $\langle GT\rangle$ with $L_{1A} = 0$, Z_d refers to numerical results with the Z-parameterization: $\rho_t' = 0.69/\gamma_t$.

	$\langle GT\rangle$	$\langle GT\rangle$, Z_d
1-body LO,$\alpha = 0$	$\sqrt{3}$	$\sqrt{3}$
1-body LO, $\alpha = 0$, $a_{np} \neq a_{pp}$	1.722	1.723
1-body LO	1.657	1.668
1-body NLO	1.6215	1.602
Full NLO $L_{1A} = 0$, $\alpha = 0$	1.7146	1.699
Full NLO,$L_{1A} = 0$, $\alpha = 0$, $a_{np} \neq a_{pp}$	1.6979	1.6887
Full NLO $L_{1A} = 0$	1.6755	1.6585

TABLE III. Numerical calculation for $\langle GT\rangle$, Z_d refers to numerical results with the Z-parameterization: $\rho_t' = 0.69/\gamma_t$. Note that the entries with $\alpha = 0$, $a_{np} \neq a_{pp}$ comment are without explicit Coulomb force ($\alpha = 0$), but with isospin breaking in the scattering lengths, *i.e.*, the physical values with $a_{np} \neq a_{pp}$.

6. *Empirical extraction of Gamow-teller strength and fixing L_{1A}.*

The GT matrix element can extracted using eq. (103). The axial coupling constant g_A has been remeasured recently, giving results whose range is much bigger than the current recommendation. To be on the safe side, we take $g_A = 1.273 \pm 0.003 \pm 0.005$ [52, 53]. The first uncertainty in g_A arises from the the difference between the measurements of Refs. [52, 53], and the second uncertainty is the statistical experimental uncertainty. In order to extract the Gamow-Teller strength, we use $\langle F\rangle$ is the Fermi transition taken from Fig. 17. At infinity we find that the empirical GT strength is $\langle GT\rangle_{\rm emp} = \sqrt{3}\frac{1.213\pm0.002}{g_A}$. The uncertainty here originates mainly from the uncertainty in the triton half-life.

The difference between the empirical GT strength and the numerical result for the GT-transition at NLO is used to fix L_{1A} for ERE or Z-parameterization. Importantly, we find numerically in both cases, that the following combinations are RG invariant, a fact that was predicted by theory [25]:

$$M\frac{L_{1A}^{ERE}\left(\mu - \frac{1}{a_s}\right)\left(\mu - \frac{1}{a_t}\right)}{4\pi g_A} = 0.99 \pm 0.2 \pm 0.2 \tag{123}$$

$$M\frac{L_{1A}^{Z_d}\left(\mu - \frac{1}{a_s}\right)\left(\mu - \frac{1}{a_t}\right)}{4\pi g_A} = 0.24 \pm 0.2 \pm 0.2 \tag{124}$$

The first uncertainty comes from the aforementioned difference between recent experimental determinations of g_A [52, 53], and the second uncertainty comes from the rest of the experimental uncertainties, such as the statistical in the measured triton half-life.

7. *Theoretical uncertainty in the decay calculation*

The approach used here, like any other EFT, is useful for robust and reliable theoretical uncertainty estimates,

due to neglected orders in the EFT expansion. Let us first note the following points:

Renormalization:- In chiral nuclear effective theory, cutoff variation is frequently used to obtain an uncertainty estimate for a calculation. A main advantage of our approach is that we achieved cutoff invariance through order-by-order renormalization. This cutoff independence persists at cutoffs much larger than the breakdown scale. This implies that our remaining uncertainties are free from regularization artifacts. We show that such regulator effects can be sizable up to cutoff larger than the naïve breakdown scale $\mu = m_\pi$. Note that RG invariance does not result in a reduction of the intrinsic error of the EFT. However, it provides also an additional test of our calculation. For example, we reproduce the theoretically predicted cutoff dependence of L_{1A} numerically.

Perturbation theory:- We use a consistent perturbative approach. This allows us to use the ratio of the next-to-leading contribution to the leading order result, as a measure of the uncertainty in our calculation. As an even more robust estimate, we study the contributions of the different NLO terms. From Tab. III, one observes that while the total NLO contribution is about 1% of the LO contribution, different terms in NLO can reach 3%. We conclude that higher orders have a minor, less than 1%, effect on the triton half-life calculation.

Different arrangements of the EFT expansion:- An additional way to estimate the size of higher order corrections is by the difference between the Z-parameterization and ERE, which are both reasonable arrangements of the EFT expansion. This difference amounts to about 1% (in the observable), supporting the uncertainty estimates from the perturbation theory analysis.

Effect of electromagnetism:- Our calculation shows that this effect amounts to only 3%, split between the effect on proton-proton scattering length, and the effect of the Coulomb repulsion. Thus, even the effect of electromagnetism, which we of course included in our calculation exactly, is a rather small perturbation.

Concluding, the theoretical uncertainties due to the fact that we truncate the expansion at NLO should be of the order of 1% in the half-life of the triton. For predictions, one can use the difference between the results using the different NLO arrangements, *i.e.*, between ERE and Z-parameterization.

VIII. COMPARISON TO PREVIOUS EXTRACTIONS OF L_{1A}

L_{1A} is the only counterterm that appears in the pionless description of axial-vector electroweak reactions in nuclear two-body systems, up to fifth order [26]. This counterterm limits therefore currently the accuracy of $\not\pi$EFT calculations of the proton-proton weak fusion rate, which is the initial reaction in the *pp*-chain, *i.e.* the energy producing reaction network in stars similar to the Sun. As a result, its determination has attracted much attention in the literature.

Two main approaches were taken in previous studies to match L_{1A}. In the first, an experimental value of a two-body weak interaction process, usually at a cutoff of $\mu = m_\pi$ was used for matching. Among these reactions are deuteron dissociation by anti-neutrinos from reactors [54], and neutrino reactions with the deuteron, as measured in SNO [55], both lead to similar RG invariant combinations of the two-body axial strength, $M\dfrac{L_{1A}\left(\mu-\frac{1}{a_s}\right)\left(\mu-\frac{1}{a_t}\right)}{4\pi g_A} \approx 0.4 \pm 0.8$. In both cases, the large error bar originates from statistical errors in the experiments, due to the small cross section for neutrino-deuteron reactions. The authors of Ref. [27] proposed therefore a precision measurement of muon capture on the deuteron, with the aim of reducing the error bar by a factor of 3, reflecting an estimated 2-3% experimental uncertainty in the (then proposed) ongoing MuSun experiment [56]. It is important to note that the $\mu - d$ capture has a large energy transfer, possibly too large for an application of $\not\pi$EFT , which will clearly impact the convergence pattern of any calculation. In all these, the uncertainties are mainly experimental, due to the uncertainty in the observable.

A different approach was taken by Ando and collaborators in Ref. [28]. They used the hybrid calculation of the proton-proton fusion rate from Ref. [22]. As a constraint, they took from that calculation the ratio of the two-body strength over the one-body strength, and matched L_{1A} to reproduce this ratio in the $\not\pi$EFT regime. Their result was $M\dfrac{L_{1A}\left(\mu-\frac{1}{a_s}\right)\left(\mu-\frac{1}{a_t}\right)}{4\pi g_A} = 0.1965 \pm 0.005$. The small error bar here is due to the accurate triton half-life measurement that is used to fix undetermined counterterms in Ref. [22]. However, our work highlights a few criticisms of Ref. [28]. Firstly, a three-body constraint should be taken at a sufficiently large cutoff, to make sure no regularization effects affect the cutoff invariance. Secondly, they take a phenomenological approach which leads to contributions from higher orders to the NLO calculation, as they take the nonperturbative Z_d at all orders. These two reasons entail that a robust theoretical uncertainty estimate is very hard within this approach, and indeed it is missing from the L_{1A} result in this case. Lastly, and most importantly, the constraint they take is not an observable, as one can use hermitian transformations to shift strengths from the two-body sector to the one-body, and vice versa.

IX. SUMMARY AND OUTLOOK

In this paper we have studied tritium β-decay in the framework of the pionless effective field theory up to next-to-leading order. This was done by establishing a perturbative and consistent framework to calculate tran-

sitions between three-body bound states, up to NLO. Our method is based on a diagrammatic expansion of both the nuclear amplitudes (wave functions) and the matrix elements.

In our calculation we used that matrix elements can be calculated diagrammatically by summing all possible insertions of the transition operator between two nuclear amplitudes. At LO, we showed that this is consistent with the Bethe-Salpeter normalization condition, its diagrammatic representation is equivalent to summing of all possible insertions between to identical bubbles.

At NLO, we used that a consistent diagrammatic expansion is just the sum of all possible diagrams with a single NLO perturbation insertion. We obtained the NLO wave function normalization from the residue of the NLO scattering amplitude.

The LO and NLO three-nucleon (^{3}H and ^{3}He) amplitudes were calculated as solutions of the homogeneous Faddeev equations. At NLO, these solutions require a recalibration of the three-body force $(H^1(\Lambda), H^\alpha(\Lambda))$ reproducing the results of Ref. [17, 47]

Using a diagrammatic approach we calculated the β-decay of ^{3}H into ^{3}He at NLO. This reaction depends on two operators, the Fermi transition, which includes a one-body polar-vector part, and the Gamow-Teller transition, which includes one- and two-body axial-vector parts.

We have tested the correct renormalization of our perturbative calculation of the Fermi and Gamow-Teller transitions by an analysis of the residual cutoff dependence of the matrix elements, up to very large cutoffs, significantly larger than the breakdown scale of the EFT. The numerical results for the RG invariance reproduce theoretical predictions and serve therefore as an additional test of the calculation and our approach.

We used the NLO calculation to fix the unknown NLO LEC, L_{1A}. The counterterm L_{1A} is also relevant for a high-accuracy prediction of the solar proton-proton fusion rate [23, 24, 28].

The NLO correction is about 1% for the triton decay Gamow-Teller strength. In addition we have shown that these conclusions are insensitive to different arrangements of the effective range expansion. The fact that our calculation is carried out within a consistent perturbative approach allows reliable uncertainty estimates. We find that the theoretical uncertainty on the ^{3}H decay rate is about 1%, entailing an uncertainty of about 0.5 on L_{1A}, which is of the order of the uncertainty in L_{1A} that originates from the experimental uncertainties in g_A and the half-life measurement.

As mentioned, L_{1A}, takes part in low-energy weak processes such as *pp*-fusion [23, 24, 28, 57] and muon capture [27, 58–61]. In the near future, we intend to examine our result for L_{1A} and its uncertainty by addressing these low-energy weak processes [62, 63].

In addition, we plan to use the approach outlined here, to calculate perturbatively and consistently other bound state transitions, up to NLO in the pionless EFT, such as low-energy electromagnetic transitions, magnetic moments and radiative capture reactions.

ACKNOWLEDGMENT

We thank Sebastian König for the detailed comparison of the ^{3}He wave functions. We also thank Jared Vanasse, and Johannes Kirscher, as well as the rest of the participants of the GSI-funded EMMI RRTF workshop ER15-02: Systematic Treatment of the Coulomb Interaction in Few-Body Systems, for valuable discussions which have contributed us significantly in completing this work. The research of D.G. and H.D. was supported by ARCHES and by the ISRAEL SCIENCE FOUNDATION (grant No. 1446/16). The research of L.P. was supported by the National Science Foundation under Grant Nos. PHY-1516077 and PHY-1555030, and by the Office of Nuclear Physics, U.S. Department of Energy under under Contract No. DE-AC05-00OR2272

APPENDIX A - NORMALIZATION OF THREE-BODY BETHE-SALPETER WAVE FUNCTIONS

In order to normalize the three-body Bethe-Salpeter (BS) wave Function we are following Refs. [38, 64, 65] and extend the derivation for the a three-body wave function.

In general the non-relativistic Bethe-Salpeter wave Function is defined [40, 64, 65]:

$$\mathcal{M} = V - VG_{BS}\mathcal{M} = V - \mathcal{M}G_{BS}V, \qquad \text{(A-125)}$$

where V is the two-body interaction kernel and G_{BS} is the free two-body propagator. From eq. (A-125) we find:

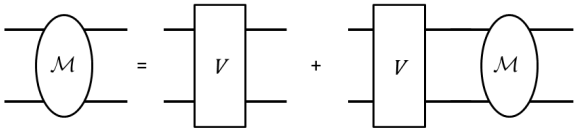

FIG. A.19. Diagrammatic representation of the two-body BS equation for the scattering matrix.

$$V = \mathcal{M} + \mathcal{M}G_{BS}V, \qquad \text{(A-126)}$$

and

$$\mathcal{M} = V - \mathcal{M}G_{BS}\mathcal{M} - \mathcal{M}G_{BS}VG_{BS}\mathcal{M}. \qquad \text{(A-127)}$$

If $\mathcal{M}$ has a bound state:

$$\mathcal{M} = \frac{|\Gamma\rangle\langle\Gamma|}{E - E_B}, \qquad \text{(A-128)}$$

where $|\Gamma\rangle$ is wave function amplitude and $\langle\Gamma|$ is the representation of $|\Gamma\rangle$ in the dual space, including Dirac conjugation. The first term is the contribution from the

bound state propagator, with possible spin degrees of freedom associated with the propagation of the bound state suppressed, Substituting eq. (A-128) into the linear form (eq. (A-125)) of the equation for $\mathcal{M}$, and equating residues at $E = E_B$ gives the wave equation for the vertex function $|\Gamma\rangle$:

$$|\Gamma\rangle = VG_{BS}\,|\Gamma\rangle\,. \tag{A-129}$$

By substituting eq. (A-128) into eq. (A-127) we get for $E = E_B$:

$$\begin{aligned}|\Gamma\rangle\langle\Gamma| &= -\lim_{E\to E_B}|\Gamma\rangle\frac{\langle\Gamma|\,G_{BS}\,(1+VG_{BS})\,|\Gamma\rangle}{E-E_B}\langle\Gamma| \\ &= -\lim_{E\to E_B}\frac{\langle\Gamma|\,G_{BS}\,(1+VG_{BS})\,|\Gamma\rangle}{E-E_B} = \\ &-\lim_{E\to E_B}\frac{\langle\Gamma|\,G_{BS}\left(G_{BS}^{-1}+V\right)G_{BS}|\Gamma\rangle}{E-E_B}.\end{aligned} \tag{A-130}$$

Since $\lim_{E\to E_B}\langle\Gamma|\,G_{BS}\,(1+VG_{BS})\,|\Gamma\rangle = 0$ After some algebra (see [38] for more details) eq. (A-130) becomes:

$$1 = -\frac{\langle\Gamma|\,G_{BS}\partial\left(G_{BS}^{-1}+V\right)G_{BS}\,|\Gamma\rangle}{\partial E}|_{E=E_B}. \tag{A-131}$$

In our notation:

$$G_{BS} = \mathcal{D} \tag{A-132}$$

$$V = \mathcal{K} \tag{A-133}$$

[1] P. F. Bedaque and U. van Kolck, Ann. Rev. Nucl. Part. Sci. **52**, 339 (2002), arXiv:nucl-th/0203055 [nucl-th].
[2] D. B. Kaplan, M. J. Savage, and M. B. Wise, Nucl. Phys. **B478**, 629 (1996), arXiv:nucl-th/9605002 [nucl-th].
[3] D. B. Kaplan, M. J. Savage, and M. B. Wise, Nucl. Phys. **B534**, 329 (1998), arXiv:nucl-th/9802075 [nucl-th].
[4] D. B. Kaplan, M. J. Savage, and M. B. Wise, Phys. Lett. **B424**, 390 (1998), arXiv:nucl-th/9801034 [nucl-th].
[5] D. B. Kaplan, M. J. Savage, and M. B. Wise, Phys. Rev. **C59**, 617 (1999), arXiv:nucl-th/9804032 [nucl-th].
[6] E. Epelbaum, H.-W. Hammer, and U.-G. Meissner, Rev. Mod. Phys. **81**, 1773 (2009), arXiv:0811.1338 [nucl-th].
[7] S. Bacca and S. Pastore, J. Phys. **G41**, 123002 (2014), arXiv:1407.3490 [nucl-th].
[8] D. R. Phillips, Annual Review of Nuclear and Particle Science **66**, 421 (2016), http://dx.doi.org/10.1146/annurev-nucl-102014-022321.
[9] H. W. Griesshammer, Nucl. Phys. **A760**, 110 (2005), arXiv:nucl-th/0502039 [nucl-th].
[10] L. Platter, Few Body Syst. **46**, 139 (2009), arXiv:0904.2227 [nucl-th].
[11] P. F. Bedaque, H.-W. Hammer, and U. van Kolck, Nucl. Phys. **A646**, 444 (1999), arXiv:nucl-th/9811046 [nucl-th].
[12] P. F. Bedaque, H.-W. Hammer, and U. van Kolck, Nucl. Phys. **A676**, 357 (2000), arXiv:nucl-th/9906032 [nucl-th].
[13] G. Rupak and X.-W. Kong, Nucl. Phys. **A717**, 73 (2003), arXiv:nucl-th/0108059 [nucl-th].
[14] S.-I. Ando and M. C. Birse, J. Phys. **G37**, 105108 (2010), arXiv:1003.4383 [nucl-th].
[15] J. Kirscher and D. Gazit, Physics Letters B **755**, 253 (2016), arXiv:1510.00118 [nucl-th].
[16] S. Koenig and H.-W. Hammer, Phys. Rev. **C83**, 064001 (2011), arXiv:1101.5939 [nucl-th].
[17] J. Vanasse, D. A. Egolf, J. Kerin, S. Koenig, and R. P. Springer, Phys. Rev. **C89**, 064003 (2014), arXiv:1402.5441 [nucl-th].
[18] S. Koenig, H. W. Grießhammer, and H. W. Hammer, J. Phys. **G42**, 045101 (2015), arXiv:1405.7961 [nucl-th].
[19] E. G. Adelberger *et al.*, Rev. Mod. Phys. **83**, 195 (2011), arXiv:1004.2318 [nucl-ex].
[20] R. Schiavilla, V. G. J. Stoks, W. Glöckle, H. Kamada, A. Nogga, J. Carlson, R. Machleidt, V. R. Pandharipande, R. B. Wiringa, A. Kievsky, S. Rosati, and M. Viviani, Phys. Rev. C **58**, 1263 (1998).
[21] D. Gazit, S. Quaglioni, and P. Navrátil, Phys. Rev. Lett. **103**, 102502 (2009).
[22] T.-S. Park, L. E. Marcucci, R. Schiavilla, M. Viviani, A. Kievsky, S. Rosati, K. Kubodera, D.-P. Min, and M. Rho, Phys. Rev. C **67**, 055206 (2003).
[23] X. Kong and F. Ravndal, Nucl. Phys. **A656**, 421 (1999), arXiv:nucl-th/9902064 [nucl-th].
[24] X. Kong and F. Ravndal, Phys. Rev. **C64**, 044002 (2001), arXiv:nucl-th/0004038 [nucl-th].
[25] M. Butler and J.-W. Chen, Nuclear Physics A **675**, 575 (2000), nucl-th/9905059.
[26] M. Butler and J.-W. Chen, Physics Letters B **520**, 87 (2001).
[27] J.-W. Chen, T. Inoue, X.-d. Ji, and Y.-c. Li, Phys. Rev. **C72**, 061001 (2005), arXiv:nucl-th/0506001 [nucl-th].
[28] S. Ando, J. W. Shin, C. H. Hyun, S. W. Hong, and K. Kubodera, Phys. Lett. **B668**, 187 (2008), arXiv:0801.4330 [nucl-th].
[29] See also a recent study using lattice EFT, published online at the finishing stages of preparation of the current mansucript, M. J. Savage, P. E. Shanahan, B. C. Tiburzi, M. L. Wagman, F. Winter, S. R. Beane, E. Chang, Z. Davoudi, W. Detmold, and K. Orginos, ArXiv e-prints (2016), arXiv:1610.04545 [hep-lat].
[30] S. R. Beane and M. J. Savage, Nucl. Phys. **A694**, 511 (2001), arXiv:nucl-th/0011067 [nucl-th].
[31] D. B. Kaplan, M. J. Savage, and M. B. Wise, Phys. Lett. **B424**, 390 (1998), arXiv:nucl-th/9801034 [nucl-th].
[32] H. W. Griesshammer, Nucl. Phys. **A744**, 192 (2004), arXiv:nucl-th/0404073 [nucl-th].
[33] D. R. Phillips, G. Rupak, and M. J. Savage, Phys. Lett. **B473**, 209 (2000), arXiv:nucl-th/9908054 [nucl-th].
[34] J. Vanasse, Phys. Rev. **C88**, 044001 (2013), arXiv:1305.0283 [nucl-th].
[35] J. Vanasse, (2015), arXiv:1512.03805 [nucl-th].
[36] X. Kong and F. Ravndal, Nucl. Phys. **A665**, 137 (2000), arXiv:hep-ph/9903523 [hep-ph].
[37] X. Kong and F. Ravndal, Phys. Lett. **B450**, 320 (1999),

arXiv:nucl-th/9811076 [nucl-th].
[38] S. König, *Effective quantum theories with short- and long-range forces*, Ph.D. thesis, Universität Bonn, Germany (2013).
[39] M. Blank and A. Krassnigg, Comput. Phys. Commun. **182**, 1391 (2011), arXiv:1009.1535 [hep-ph].
[40] C. L. Smith, Annals of Physics **53**, 521 (1969).
[41] S. König, "Low-energy p–d scattering and 3he in pionless eft," (2012), slides of a talk given at the Triangle Nuclear Theory Seminar Duke University, Durham, NC.
[42] C. Van Der Leun and C. Alderliesten, Nucl. Phys. **A380**, 261 (1982).
[43] J. J. de Swart, C. P. F. Terheggen, and V. G. J. Stoks, *3rd International Symposium on Dubna Deuteron 95 Dubna, Russia, July 4-7, 1995*, (1995), arXiv:nucl-th/9509032 [nucl-th].
[44] S. R. Beane, P. F. Bedaque, W. C. Haxton, D. R. Phillips, and M. J. Savage, "From Hadrons to Nuclei: Crossing the Border," in *At the Frontier of Particle Physics: Handbook of QCD (in 3 Vols). Edited by SHIFMAN M. Published by World Scientific Publishing Co. Pte. Ltd., 2001. ISBN #9789812810458, pp. 133-269*, edited by M. Shifman (World Scientific Publishing Co, 2001) pp. 133–269.
[45] J. R. Bergervoet, P. C. van Campen, W. A. van der Sanden, and J. J. de Swart, Phys. Rev. **C38**, 15 (1988).
[46] S. Koenig, H. W. Grießhammer, H.-W. Hammer, and U. van Kolck, J. Phys. **G43**, 055106 (2016), arXiv:1508.05085 [nucl-th].
[47] C. Ji, D. R. Phillips, and L. Platter, Annals of Physics **327**, 1803 (2012), arXiv:1106.3837 [nucl-th].
[48] C. Ji and D. R. Phillips, Few Body Syst. **54**, 2317 (2013), arXiv:1212.1845 [nucl-th].
[49] Yu. A. Akulov and B. A. Mamyrin, Phys. Lett. **B610**, 45 (2005).
[50] J. C. Hardy, I. S. Towner, V. T. Koslowsky, E. Hagberg, and H. Schmeing, Nucl. Phys. **A509**, 429 (1990).
[51] J. J. Simpson, Phys. Rev. **C35**, 752 (1987).
[52] S. Eidelman *et al.* (Particle Data Group), Phys. Lett. **B592**, 1 (2004).
[53] S. Pastore, F. Myhrer, and K. Kubodera, Phys. Rev. **C88**, 058501 (2013), arXiv:1309.4425 [nucl-th].
[54] M. Butler, J.-W. Chen, and P. Vogel, Physics Letters B **549**, 26 (2002), nucl-th/0206026.
[55] J.-W. Chen, K. M. Heeger, and R. G. H. Robertson, Phys. Rev. C **67**, 025801 (2003).
[56] V. A. Andreev *et al.* (MuSun), (2010), arXiv:1004.1754 [nucl-ex].
[57] E. G. Adelberger *et al.*, Rev. Mod. Phys. **70**, 1265 (1998), arXiv:astro-ph/9805121 [astro-ph].
[58] L. E. Marcucci and M. Piarulli, *International Workshop on Relativistic Description of Two- and Three-body Systems in Nuclear Physics Trento, Italy, October 19-23, 2009*, Few Body Syst. **49**, 35 (2011), arXiv:1009.4016 [nucl-th].
[59] P. Ackerbauer *et al.*, Phys. Lett. **B417**, 224 (1998), arXiv:hep-ph/9708487 [hep-ph].
[60] D. Gazit, *Particles and nuclei. Proceedings, 18th International Conference, PANIC08, Eilat, Israel, November 9-14, 2008*, Nucl. Phys. **A827**, 408C (2009), [,618(2009)], arXiv:0901.0575 [nucl-th].
[61] D. Gazit, Phys. Lett. **B666**, 472 (2008), arXiv:0803.0036 [nucl-th].
[62] L. E. Marcucci, R. Schiavilla, and M. Viviani, Phys. Rev. Lett. **110**, 192503 (2013).
[63] B. Acharya, B. Carlsson, A. Ekström, C. Forssén, and L. Platter, Physics Letters B **760**, 584 (2016).
[64] R. E. Cutkosky and M. Leon, Phys. Rev. **135**, B1445 (1964).
[65] J. Adam, Jr., F. Gross, C. Savkli, and J. W. Van Orden, Phys. Rev. **C56**, 641 (1997), arXiv:nucl-th/9702014 [nucl-th].